6-2018

Loss of function of Gene X protects against α-dicarbonyl stress through the skn-1 pathway in C. elegans

Austin Lim
Dominican University of California

https://doi.org/10.33015/dominican.edu/2018.bio.07

Loss of function of *Gene X* protects against α-dicarbonyl stress through the *skn-1* pathway in *C. elegans*

By

Austin S. Lim

A culminating thesis submitted to the faculty of Dominican University of California in partial fulfillment of the requirements for the degree of Master of Science in Biology

San Rafael, California

June, 2018

This thesis, written under the direction of candidate's thesis advisor and approved by the thesis committee and the MS Biology program director, has been presented and accepted by the Department of Natural Sciences and Mathematics in partial fulfillment of the requirements for the degree of Master of Science in Biology at Dominican University of California. The written content presented in this work represent the work of the candidate alone.

Austin Lim Candidate	6/18/2018
Pankaj Kapahi, Ph.D. First Reader	6/20/2018
Wolfgang Schweigkofler, PhD. Second Reader	6/20/2018
Meredith Protas, Ph.D. Graduate Program Director	6/25/2018

Table of contents

List of Tables

List of Figures

Abstract:

Diabetes and Parkinson's Disease (PD) are on the rise worldwide. One potential contributing cause of these diseases is the accumulation of advanced glycation end products (AGEs). AGEs are a diverse group of highly oxidative byproducts produced from α-dicarbonyl compounds (α-dcs), which are regulated by a conserved glyoxalase system (*GLO1* and *DJ1*) in humans. To evaluate the role of the glyoxalase system as a key regulator of α-dcs, we utilized a *Caenorhabditis elegans* model with a mutation of *glod-4* (the worm ortholog of *GLO1*) or *djr-1.1/1.2* (the worm ortholog of *DJ1*). The *C. elegans glyoxalase* mutants demonstrated phenotypes reminiscent of α-dc-related pathologies in an age-dependent manner.

In a recent review article, novel single nucleotide polymorphisms (SNPs) associated with diabetic complications in humans identified candidate genes for further study. Through an unbiased RNAi screen on phenotypes such as lifespan and hyperesthesia utilizing the worm orthologs of the genes that the human SNPs were located in, we identified *Gene X*. *Gene X* rescued the α-dc pathologies present in the *glod-4* mutant. The key mechanism of how *Gene X* rescues these α-dc phenotypes is currently not known. Previous works shows that *Gene X* functions as a transcriptional repressor of gene expression *in vitro*. We aimed to identify through phenotypic assays and *in silico* methods how *Gene X* acts as a potential repressor for the glyoxalase regulator pathway through the *skn-1* gene. The ultimate goal of our work is to use the information about *Gene X*'s mechanistic action to open up potential treatments to alleviate α-dcs pathologies, primarily diabetic complications and Parkinson's Disease.

To examine the mechanistic actions of *Gene X* in *C. elegans*, we had the following aims:

Aim 1: Study the role of *Gene X* in mediating α-dicarbonyl/AGEs in the *C. elegans* model of long-term diabetic complications.

- Aim 1.1: Investigate whether *Gene X* knockout mutants are able to rescue the short lifespan of glyoxalase mutants.
- Aim 1.2: Through the utilization of *Gene X* mutants, examine if there is a rescue effect for the multiple models of neurodegeneration (pan-neuronal, Dopaminergic, and α-synuclein).

Aim 2: Characterizing the mechanism of *Gene X* in *C. elegans.*

- Aim 2.1: Investigate *in silico* the binding sites of *Gene X* in *C. elegans*.
- Aim 2.2: Identify gene expression differences in the glyoxalase pathway that are altered between the *Gene X* mutant and the wildtype.
- Aim 2.3: Identify the role of the *skn-1* gene in the glyoxalase regulation pathway.

Acknowledgements

I would like to thank the following people for their contribution to the creation and completion of this body of work. The following are from the Buck Institute for the Research of Aging: Pankaj Kapahi, PhD., for accepting me into his lab and providing guidance. Sanjib Guha, PhD., for being my mentor and for his unending support in helping me develop as a scientist, develop our experimental design, and learn the assays to complete this body of work. David Hall, Jyotiska Chaudhuri, PhD., Manish Chamoli, PhD., and Jianfeng Lan, PhD., for helping me learn the original protocols for maintenance of my model organisms, leading to experimental design. Kenny Wilson, PhD., for his continued contributions in the betterment of this manuscript. I would like to thank the following people from Dominican University of California: Wolfgang Schweigkofler, PhD., Meredith Protas, PhD., and Maggie Louie, PhD., also for helping with the writing, completion of this manuscript, and organization of the M.S. program. Furthermore I would like to thank my family for their unending support and guidance during this time as a Master's student.

Introduction:

Age and disease:

Aging is a complex process that regulates multiple biological interactions over time to impact an individual's lifespan and healthspan (1). The number of individuals over the age of 60 has been steadily increasing with the estimated number of people world-wide affected around 900 million (2,3). With the expansion of the older population, a multitude of age-related diseases (Figure 1) are also on the rise leading to a reduction in quality of life (1). One age-related disease that has been slowly increasing in prevalence and predicted to double in the next 20 years with the aging population is diabetes (4). Diabetes is caused by hyperglycemia (a condition where blood glucose levels are significantly higher than normal levels of 200 mg/dL (5)) and insulin resistance, which is due to the bodies inability to process dietary glucose (6). There are two types of diabetes. Type 1 patients experience insulin deficiency due to the destruction of pancreatic cells by their immune system, thus

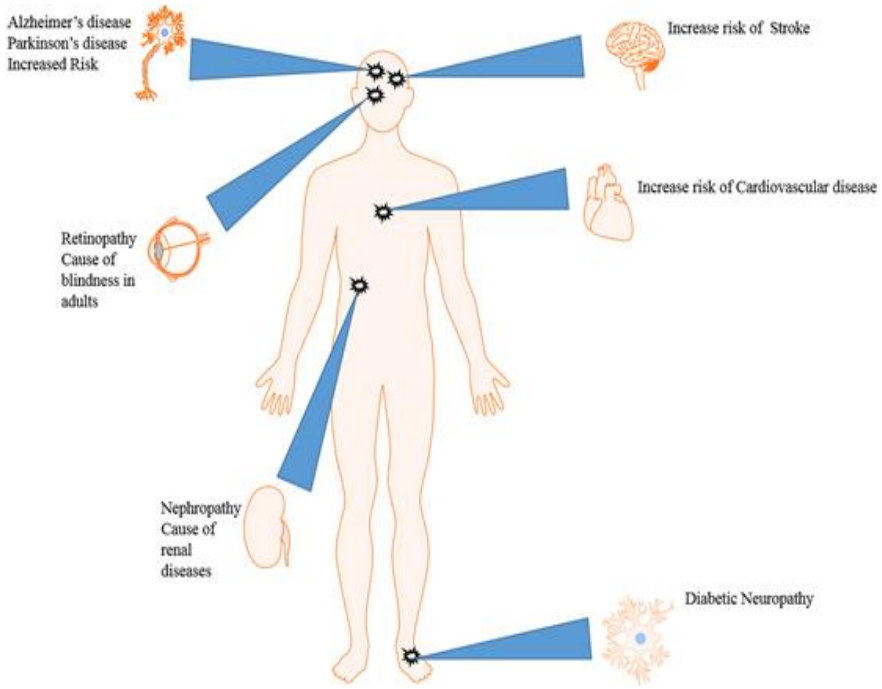

Figure 1: **Overview of diabetes associated complications.** Information from Van Den Born et al., Diabetes, 2016

hindering their production of insulin (7). Type 2 diabetes is less understood but it has been shown that in obese individuals, cells develop insulin resistance which results in the demand for increased insulin production (8). Pancreatic cells are unable to produce enough insulin to meet this demand, resulting in diabetes. Left untreated, diabetes causes people to suffer from complications such as touch sensitivity (also called neuropathy), increased risk of stroke, and mortality (Figure 1) (6). Scientists have recently observed that in long-term diabetic patients there is an elevated risk to age-related diseases such as neurodegenerative diseases (9). As the risk of diabetic complications increased, disease phenotypes such as diabetic neuropathy and neuronal damages also increased due to the loss and impairment of neurotrophic support (10,11), such as reduction in the nerve growth factor neurotrophin-3. To better understand why there is such a connection, scientists are now evaluating potential causes within these mechanisms that could regulate both diabetes and neurodegenerative disorders (9).

Neurodegenerative diseases like Alzheimer's disease and Parkinson’s Disease (PD) affect millions of people worldwide (12). These diseases impair an individual's ability to move or mentally function (13) due to the slow and progressive loss of neurons and axons within the nervous system (14). In order to understand these diseases, scientists are now evaluating the biological mechanisms and signals that are driving these processes of age-related decline (15).

Scientists hypothesize that one mechanism which triggers neuronal degeneration in the central nervous system is chronic inflammation (16). Long term chronic inflammation upregulates cytokine and interleukins production, leading to the inhibition of natural homeostasis feedback mechanisms. This, in turn, causes toxic effects in the

body (17). The inflamed cells become permeable, allowing leukocytes to enter the neurons and leading to the production of protein aggregates. Protein aggregation continues to trigger inflammation, as the immune system believes that the aggregates are an infection. In turn, this leads to the production of oxidative stress.

Advance Glycation End products (AGEs) formation:

Recent studies have shown that oxidative stress is a key factor which contributes to neurodegeneration (18). Scientists have found that high levels of reactive oxygen species (ROS) are associated with oxidative stress, which in turn leads to the modification of biological molecules, the impairment of biological processes, and ultimately cell death. Examples of reactive oxidative species are advanced glycation end products (AGEs).

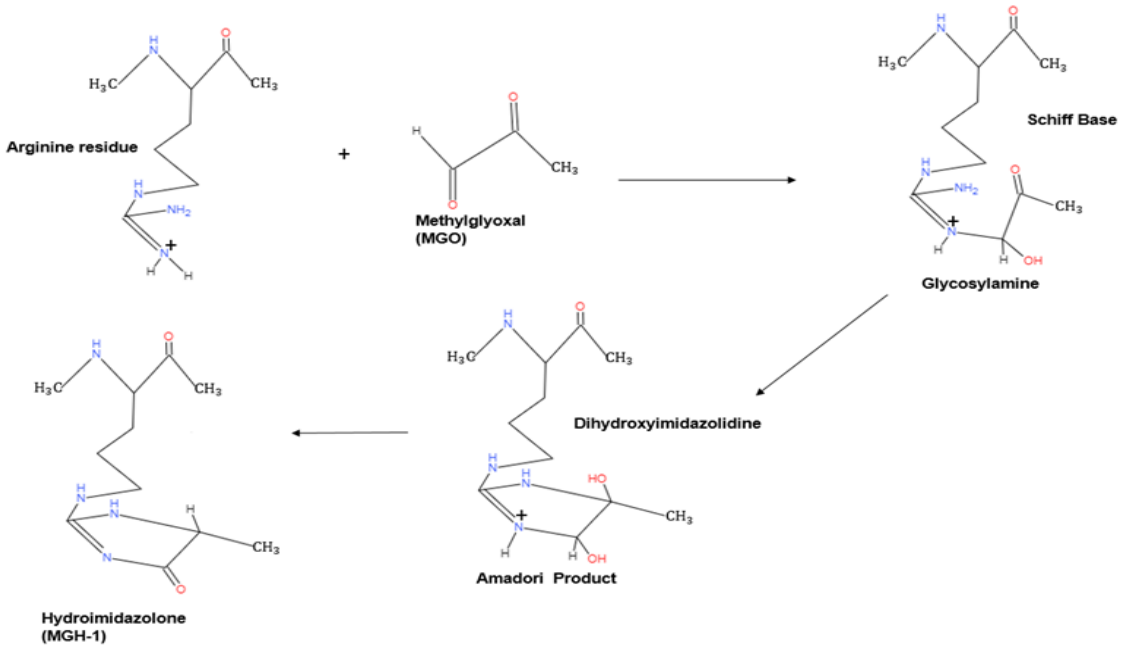

Figure 2: **AGE formation e.g. Hydroimidazolone (MGH-1)** through the association to Arginine residue. Maillard reaction occurs to create Schiff base, which undergoes Amadori rearrangement to reactive species AGE. Modified with permission from Rabbani N, Thornalley PJ. Biochem Biophys Res Commun. (2015)

AGEs are toxic molecules that are seen in a multitude of diseases such as diabetes, inflammation, and renal failure (19). AGEs are byproducts created through lipid peroxidation and glycolysis. They are created from a Maillard reaction which leads to a non-enzymatic formation of a Schiff base and enzymatic intermediates created from free amino acids binding to the sugar. Schiff bases either undergo a rearrangement within itself (20) or participate in an Amadori rearrangement reaction with a protein amino group to become AGEs (Figure 2) (21). These molecules then react with receptors (known as RAGEs), which activate a cascade of inflammatory responses that are detrimental to the body in the long term. To understand AGEs and how they impact

neurodegenerative disorders through RAGEs, scientists are now examining the precursor α-dicarbonyl compounds (α-dcs) for AGEs (22–24).

α-dcs are highly reactive and are associated with multiple pathologies such as diabetes (25) as well as neurodegenerative diseases such as Parkinson's (26). α-dcs are byproducts made during the glycolysis process as the cells degrade glyceraldehyde-3-phospate (GA3P) as well as dihydroxyacetonephosphate (DHAP) (27). After the creation of these reactive byproducts, α-dcs have a tendency to be very reactive, binding to proteins before the gastrointestinal lumen can absorb them, which creates more oxidative stress (27). Increased stress by α-dcs exacerbates damage in cellular functions, which in turn increases the risk of diseases (27). With the overall rise of diabetes in the population, scientists are now examining potential associations between dicarbonyl stresses and diabetic complications. In a Cohort on Diabetes and Atherosclerosis Maastricht (CODAM) study, there were elevated free α-dcs in diabetic patients with impaired glucose metabolism (IGM) from plasma that potentially increased the risk of long term damage in bodily systems (28). Because of these associations, researchers are now focusing on the detoxification pathway for these byproducts as a potential treatment option to regulate these stresses.

Conserved Glyoxalase Detoxification System:

In order to detoxify α-dcs, the body upregulates the glyoxalase GLO1 pathway (26,27,29). The detoxification pathway for these toxic byproducts primarily relies on two different enzymes. First, *GLO1* converts accumulated toxic glyolyctic byproducts into glutathione (30), which is further converted into lactate by the secondary enzyme, *GLO2*

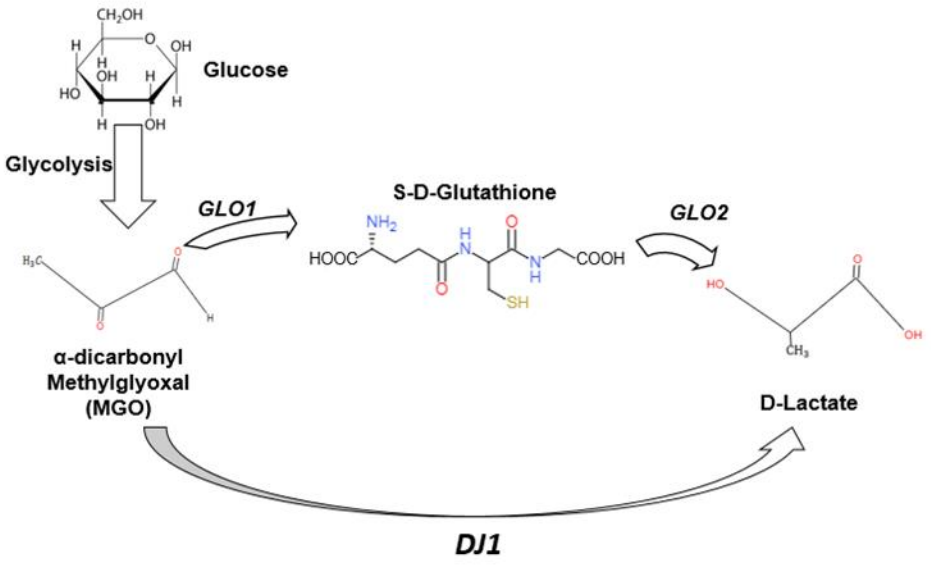

Figure 3: **Glyoxalase detoxification system for methylglyoxal formation.** Methylglyoxal is detoxified utilizing glutathione-dependent glyoxalase system (*GLO1/ GLO2*) to D-lactate. Information from Matsuda, Noriyuki et al., Science Reports, 2017 and Hasim, Sahar, Journal of Biological Chemistry, 2013

(Figure 3,(30)). In examining regulation of α-dcs, researchers have seen that as *GLO1* expression increases, the accumulation of free α-dcs radicals are decreased (31,32). Consistent with this, researchers have also noticed that in diabetic patients the expression of *GLO1* was inhibited (32). Inhibition of *GLO1* resulted in elevated levels of α-dc radicals, which increases the risk for diabetic complication (25,26,32,33).

As the frequency of diabetic complications rises, the risk of neurodegenerative diseases such as PD also rises (34). PD is a disease most commonly associated with the loss of dopaminergic neurons due to the presence of α-synuclein (35). α-synuclein accumulation leads to Lewy bodies which cause an immune reaction leading to neuronal degradation, tremors, slowness, and ultimately dementia (35,36). This deadly disease led scientists to investigate how α-synuclein is created in PD. To date, scientist have discovered multiple genes associated with PD such as *LRRK2*, *PARK2*, and *PINK1* (35). In further evaluating the genome, researchers have discovered that a gene known as *DJ1* is associated with PD and regulates oxidative stress by inhibiting α-synuclein oligomers (34). *DJ1* also functions similarly to *GLO1* through protection against glyoxal damage in diabetes (37). *DJ1* mutants in *C. elegans* and mice also had increased levels of α-dcs (37). The researchers concluded that *DJ1* functions independently as a glyoxalase, which also focuses on detoxifying the α-dcs (37). To better examine how these glyoxalases function *in vivo*, our lab is utilizing *C. elegans* as a model organism because of their efficient replication of pathological phenotypes, the presence of orthologs for *DJ1* and *GLO1*, and their relatively short lifespan (26).

***C. elegans* as a genetic model:**

C. elegans has been used as a model for the past 50 years because it allows for genetic and developmental manipulation (38). While *C. elegans* shares about 60-80% of their genome with humans, it has been determined that 40% of all previously studied proteins associate with known human diseases (39). The presence of *C. elegans* orthologs allows us to map and model potential biological processes seen in humans.

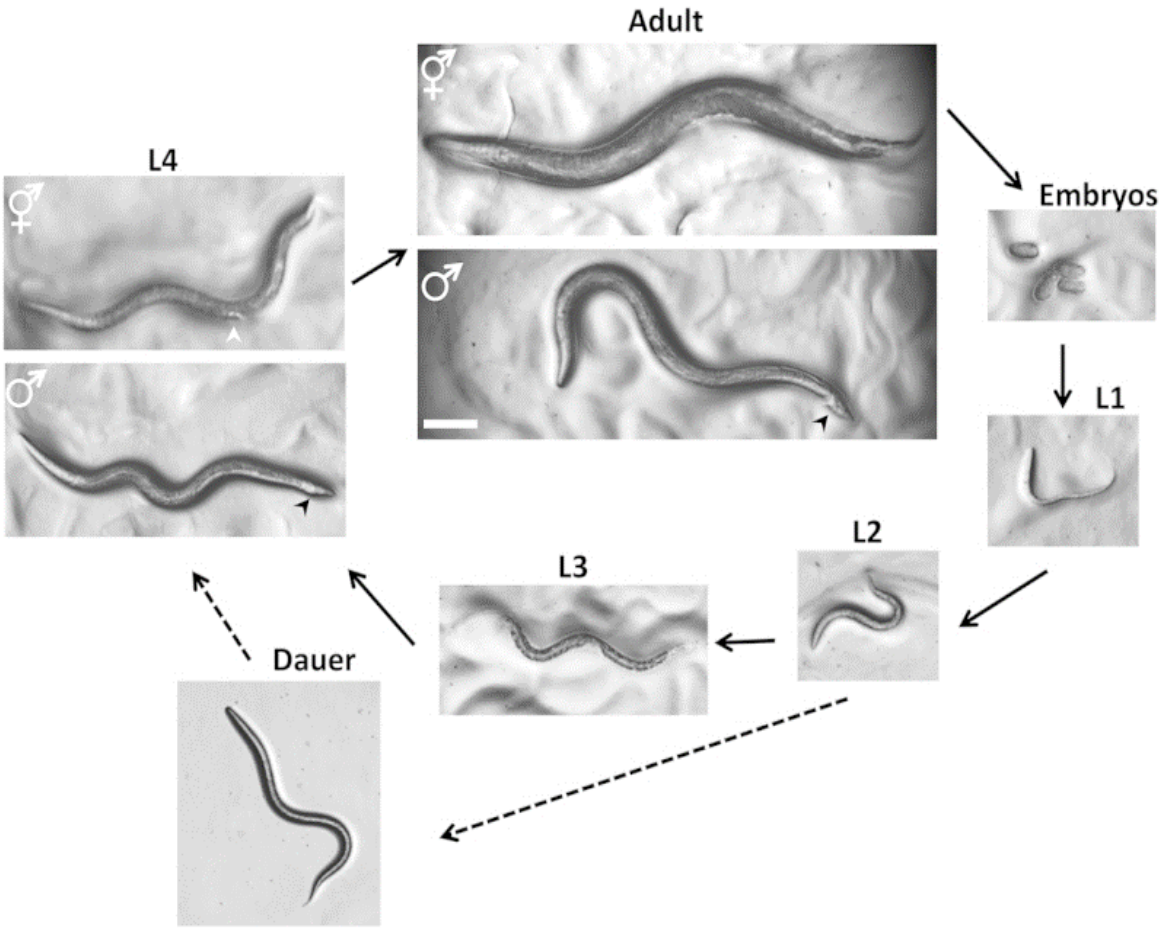

Figure 4: ***C. elegans* model life cycle form egg stage to adulthood.**

Used with permission from Ann K. Corsi, Bruce Wightman, and Martin Chalfie, Wormbook: The online Review of *C. elegans* Biology (2015)

There are also multiple ways to genetically manipulate these organisms to screen for a particular mutation or reduced genetic expression through the feeding of RNA interference (RNAi). RNAi is a genetic manipulation that scientists utilize to inhibit or knock down the expression of a particular gene. This performed in *C. elegans* through the feeding of bacteria that produced double stranded RNA, which leads to the degradation and interference of the corresponding mRNA (40). After genetic manipulation, we are able perform rapid phenotypic evaluation on these animals, due to their relatively short lifespan of three weeks (Figure 4). A nother advantage of *C. elegans* is their transparent epidermis which allows for the study of fluorescent-tagged gene expression. The Kapahi lab utilized *C. elegans* lines with mutations in *glod-4* (the *C. elegans* ortholog of *GLO1*) and *djr-1.1/1.2* (*DJ1* in humans) and determined that these mutants have difficulty detoxifying α-dcs (26), similar to human patients. In addition, mutating these glyoxalase genes led to the generation of pathological diabetic complications and neurodegeneration phenotypes (26). Modeling pathological phenotypes in *C. elegans* allowed for the discovery of a regulation pathway for these glyoxalase genes.

***trpa-1/ skn-1* pathway in *C elegans*:**

Through the modeling of pathological phenotypes, Kapahi lab has identified a *trpa-1* pathway that regulates the glyoxalase genes, which leads to the detoxification of α-dcs. *trpa-1* is known to be an ion channel that has been implicated in mechanosensory behaviors such as touch avoidance (41). Our lab found that when *trpa-1* is activated in response to accumulating α-dcs (Figure 5), p38 is activated. This signals to the downstream transcription factor skinhead-1 (*skn-1*) in *C. elegans*, which in humans is

Figure 5: ***trpa-1/ skn-1*** **pathway for α-dicarbonyl detoxification**

Reprinted from Current Biology, 22, Chaudhuri, Jyotiska et al. A Caenorhabditis elegans Model Elucidates a Conserved Role for TRPA1-Nrf Signaling in Reactive α-Dicarbonyl Detoxification, 3014–25, Copyright (2016), with permission from Elsevier."

known as Nuclear factor-elytroid-related factor 2 (NRF2), to transcribe *skn-1* mRNA, which is a known longevity gene (42). This leads to further glyoxalase activation to alleviate α-dc stress. Furthermore, *skn-1* is a gene that is known to regulate multiple pathways and contributes to lifespan extension through its role in detoxifying ROS (42). In order to react to ROS and oxidative stress, *skn-1 is* phosphorylated by p38 MAPK, leading to the induction of antioxidants and detoxifying downstream targets like *gst-4* and

gcs-1 (43). These downstream targets both play a role in oxidative stress response (44,45) that has been seen to regulate the glyoxalase genes (26). Utilizing the *C. elegans* model, we previously were able to discover the role that the *skn-1* cascade plays in regulating glyoxalase expression to combat α-dcs such as methylglyoxal (MGO) (26). To further understand this new pathway in the context of disease pathologies, we looked to published literature with a focus on diabetic complications such as cardiomyopathy and nephropathy.

Novel RNAi screen using human GWAS hits:

In a recently published review, a number of novel single nucleotide polymorphisms (SNPs) associated with diabetic complications were identified through a genome-wide association screen (GWAS) (46). Before I joined, the Kapahi Lab performed a BLAST analysis to find *C. elegans* orthologs of these human genes (46). To examine if these 20 worm genes had phenotypic effects on diabetic complications, we knocked them down using RNAi in wildtype worms and *glod-4* mutants and examined lifespan and touch sensitivity. Through this screen we identified four key genes that affected lifespan and touch sensitivity, with *Gene X* rescuing the harmful effect of the *glod-4* mutation and the remaining three exacerbated the pathological phenotype (Table 1).

Table 1: List of genes with prominent phenotype in *glod-4* mutant RNAi screen utilizing the diabetic disease pathologies.

Human Gene/ RNAi sample	Lifespan	Hyperesthesia
3 fat metabolism genes	decreases	increases
Gene X	increases	decreases

Gene X is a relatively uncharacterized gene and it has not yet been shown to be associated with α-dcs. It has been previously reported to regulate chemoreceptor genes in AWC olfactory neurons by acting as a repressor for these neurons (47). In human cell lines *Gene X* plays a role similar to that in *C. elegans* and demonstrates a repressor-like effect by inhibiting Natural Killer (NK) cell's activity (48). *Gene X* also has been shown in human cancer cells to function synergistically with the alternative lengthening of telomeres (ALT) pathway to help in telomere maintenance (49). We are expanding the understanding of *Gene X* through the characterization of its potential function in the α-dc detoxification pathway.

Materials and Methods:

Strains of *C. elegans*:

Table 2: List of worm strains

Strain	Genotype	Function of strain
N2	Wildtype	mutant
Gene X	*Gene X*	mutant
glod-4	*gk189*	mutant
djr-1.1	*tm918*	mutant
djr-1.2	*tm1346*	mutant
skn-1	*zu135*	mutant
Gene X;glod-4	*Gene X; gk189*	mutant
Gene X;djr-1.1	*Gene X; tm918*	mutant
Gene X; djr-1.2	*Gene X; tm1346*	mutant
Gene X;skn-1	*Gene X; zu135*	mutant
Gene X;skn-1;glod-4	*Gene X; zu135; gk189*	mutant
OH438	*unc-4*(*e120*) II; *otIs117* IV. (*unc-33*p::GFP + *unc-4*(+))	pan-neuronal reporter
OH438; *glod-4*	*unc-4*(*e120*) II; *otIs117* IV. (*unc-33*p::GFP + *unc-4*(+)); *gk189*	pan-neuronal reporter ; mutant
OH438; *djr-1.1*	*unc-4*(*e120*) II; *otIs117* IV. (*unc-33*p::GFP + *unc-4*(+)); *tm918*	pan-neuronal reporter; mutant
OH438; *djr-1.2*	*unc-4*(*e120*) II; *otIs117* IV. (*unc-33*p::GFP + *unc-4*(+)); *tm1346*	pan-neuronal reporter ;mutant
OH438; *Gene X*	*unc-4*(*e120*) II; *otIs117* IV. (*unc-33*p::GFP + *unc-4*(+)); *Gene X*	pan-neuronal reporter; mutant
OH438; *skn-1*	*unc-4*(*e120*) II; *otIs117* IV. (*unc-33*p::GFP + *unc-4*(+)); *zu135*	pan-neuronal reporter; mutant
OH438; *Gene X ; glod-4*	*unc-4*(*e120*) II; *otIs117* IV. (*unc-33*p::GFP + *unc-4*(+)); *Gene X; gk189*	pan-neuronal reporter; mutant
OH438; *Gene X ; djr-1.1*	*unc-4*(*e120*) II; *otIs117* IV. (*unc-33*p::GFP + *unc-4*(+)); *Gene X; tm918*	pan-neuronal reporter; mutant
OH438; *Gene X ; djr-1.2*	*unc-4*(*e120*) II; *otIs117* IV. (*unc-33*p::GFP + *unc-4*(+)); *Gene X; tm1346*	pan-neuronal reporter ; mutant
OH438 ; *Gene X; skn-1*	*unc-4*(*e120*) II; *otIs117* IV. (*unc-33*p::GFP + *unc-4*(+)); *Gene X; zu135*	pan-neuronal reporter; mutant
OH438; *Gene X ; skn-1; glod-4*	*unc-4*(*e120*) II; *otIs117* IV. (*unc-33*p::GFP + *unc-4*(+)); *Gene X; zu135; gk189*	pan-neuronal reporter; mutant

Strain	Genotype	Function of strain
BY250	*vtIs7*[*Pdat-1*::GFP]	dopaminergic reporter
BY250; *glod-4*	*vtIs7*[*Pdat-1*::GFP]; *gk189*	dopaminergic reporter; mutant
BY250; *djr-1.1*	*vtIs7*[*Pdat-1*::GFP]; *tm918*	dopaminergic reporter; mutant
BY250; *djr-1.2*	*vtIs7*[*Pdat-1*::GFP]); *tm1346*	dopaminergic reporter; mutant
BY250; *Gene X*	*vtIs7*[*Pdat-1*::GFP]; *Gene X*	dopaminergic reporter; mutant
BY250; *skn-1*	*vtIs7*[*Pdat-1*::GFP]; *zu135*	dopaminergic reporter; mutant
BY250; *Gene X; glod-4*	*vtIs7*[*Pdat-1*::GFP]; *Gene X; gk189*	dopaminergic reporter; mutant
BY250; *Gene X; djr-1.1*	*vtIs7*[*Pdat-1*::GFP]; *Gene X; tm918*	dopaminergic reporter; mutant
BY250; *Gene X; djr-1.2*	*vtIs7*[*Pdat-1*::GFP]; *Gene X; tm1346*	dopaminergic reporter; mutant
BY250 ; *Gene X; skn-1*	*vtIs7*[*Pdat-1*::GFP]; *Gene X; zu135*	dopaminergic reporter; mutant
BY250; *Gene X ; skn-1; glod-4*	*vtIs7*[*Pdat-1*::GFP]; *Gene X; zu135; gk189*	dopaminergic reporter; mutant
UA44	*baIn11*(*Pdat-1*:: α-syn, *Pdat-1*::GFP)	dopaminergic reporter with α-synuclein
UA44;*glod-4*	*baIn11*(*Pdat-1*:: α-syn, *Pdat-1*::GFP); *gk189*	dopaminergic reporter with α-synuclein; Mutant
UA44; *djr-1.1*	*baIn11*(*Pdat-1*:: α-syn, *Pdat-1*::GFP); *tm918*	dopaminergic reporter with α-synuclein; mutant
UA44; *djr-1.2*	*baIn11*(*Pdat-1*:: α-syn, *Pdat-1*::GFP); *tm1346*	dopaminergic reporter with α-synuclein; mutant
UA44; Gene X	*baIn11*(*Pdat-1*:: α-syn, *Pdat-1*::GFP); *Gene X*	dopaminergic reporter with α-synuclein; mutant
UA44; skn-1	*baIn11*(*Pdat-1*:: α-syn, *Pdat-1*::GFP); *zu135*	dopaminergic reporter with α-synuclein; mutant
UA44; *glod-4; Gene X*	*baIn11*(*Pdat-1*:: α-syn, *Pdat-1*::GFP); *Gene X; gk189*	dopaminergic reporter with α-synuclein; mutant
UA44; *djr-1.1; Gene X*	*baIn11*(*Pdat-1*:: α-syn, *Pdat-1*::GFP); *Gene X; tm918*	dopaminergic reporter with α-synuclein; mutant
UA44; *djr-1.2; Gene X*	*baIn11*(*Pdat-1*:: α-syn, *Pdat-1*::GFP); *Gene X; tm1346*	dopaminergic reporter with α-synuclein; mutant
UA44 ; *Gene X; skn-1*	*baIn11*(*Pdat-1*:: α-syn, *Pdat-1*::GFP); *Gene X; zu135*	dopaminergic reporter with α-synuclein; mutant
UA44; *Gene X ; skn-1; glod-4*	*baIn11*(*Pdat-1*:: α-syn, *Pdat-1*::GFP); *Gene X; zu135; gk189*	dopaminergic reporter with α-synuclein; mutant
LD1008	*dEx9* [*skn-1*(operon)::GFP + rol-6(su1006)	translational *skn-1* operon tagged with GFP
LD1008; *Gene X*	*dEx9* [*skn-1*(operon)::GFP + rol-6(su1006); *Gene X*	translational *skn-1* operon tagged with GFP; mutant
CL2166	*dvIs19* [(pAF15)*gst-4*p::GFP::NLS])	translational *gst-4* tagged with GFP
CL2166; *Gene X*	*dvIs19* [(pAF15)*gst-4*p::GFP::NLS]); *Gene X*	translational *gst-4* tagged with GFP; mutant

Strain	Genotype	Function of strain
LD1171	*ldIs3* [*gcs-1*p::GFP + rol-6(su1006))	translational *gcs-1* tagged with GFP
LD1171 ; *Gene X*	*ldIs3* [*gcs-1*p::GFP + rol-6(su1006)); *Gene X*	translational *gcs-1* tagged with GFP; mutant

Worm Maintenance:

Strains were grown at 20˚C in a Thermo Scientific Precision incubator. Utilizing standard maintenance techniques (50), worms were fed and kept on Nematode Growth Media (NGM) seeded with fresh 5X OP50-1 *Escherichia coli*. OP50-1 was cultured in lysogeny broth overnight in a 37˚C incubator, concentrated and seeded overnight on NGM plates for use the following day. For drug assays, synchronized L4 stage worms were transferred into either 35 mm plates or 60 mm plates. Experimental plates were freshly seeded with 5X OP50-1 and; the desired drug concentration or vehicle control were placed on top of the lawn or mixed within bacteria before worms were plated. Final drug concentration was calculated by taking into account the original stock concentration and the amount of media in the NGM plate. For example, we take 70 µl of 1M MGO and seed it on a 10 ml NGM plate to create 7 mM concentration of MGO.

L1 Synchronization:

To compare the strains and pathological phenotypes, glyoxalase mutant worm populations were synchronized, using a hydrochlorite solution on a mixed population of gravid heterogeneous mothers. The hydrochlorite solution consisted of 5M KOH, 6-10% Sodium Hypochlorite, and distilled water. Worms were washed off plates using M9 buffer, centrifuged for 1 min at 2000 rpm, and supernatant removed. Next, 5 ml of hypochlorite solution was added and allowed to react up to 5 min with periodical vortexing, before centrifugation and aspiration. 5 ml of fresh M9 buffer was then added,

vortexed, and centrifuged 4 times. Worms were then suspended in 5 ml M9 buffer and shaken for 24 to 48 hours to obtain synchronized L1 stage worm population.

Worm Husbandry:

5 hermaphrodite isolates were raised on medium NGM plates with OP50-1 and incubated for 5 hours at 30˚C to heat-shock worms. After heat shock, they were returned to 20˚C and allowed to propagate. Plates were examined after 4-5 days and 20 male L4 worms were used to fertilize 4 hermaphrodites in a 60 mm plate or 10 males to 2 hermaphrodites on a 35 mm plate.

After the male plate of the strain was generated, males were crossed to L4 stage mutant lines. 10 males and 2 hermaphrodites from the mutant strain were isolated into three 35 mm plates and incubated at 15˚C for 48 hours. 6 hermaphrodites were then separated into 35mm plates and propagated at 20˚C. Next, we examined progeny of the mated mother to see if 50% of worms on the plate were males before re-isolating hermaphrodites into 30-50 35 mm plates for further propagation. PCR was used to check the genotype as follows. First worms were lysed in a solution that was 62.5% lysis buffer and 37.5% proteinase K. Next, worms are incubated in -80˚C for 15-20 minutes. Then they were ran through a thermocycler at (60˚C for 1 hour, 95˚C for 15 minutes, and 4˚C) to extract DNA. Next, the BioLabs PCR mix protocol was used (2.5 µl of Taq buffer, 0.5 µl of dNTPs mix, 0.5 µl of primers (Table 2), 0.125 µl of Taq, and 18.375-18.875 µl of water) before adding 2 µl of DNA template. The sample was run at 95˚C for 3 minutes, 95˚C for 30 seconds, 56˚C for 30 seconds, 68˚C for 1 minutes, 34 times, 68˚C for 5 minutes, and 4˚C for the glyoxalases or 95˚C for 3 minutes, 95˚C for 30 seconds, 56˚C

for 30 seconds, 68˚C for 30 seconds, 32 times, 68˚C for 5 minutes, and 4˚C for *Gene X*. Samples were run in an agarose gel with ethidium bromide to detect bands.

Table 3: PCR Primer Sequences. Internal is the sequence of the gene of interest, while external is the flanking sequences of the gene of interest

Gene Primers	**Primer Sequences**
***glod-4* internal forward**	5-CTGGTTCATTCGCGATTTTT-3
***glod-4* internal reverse**	5-CTTGAGCTCAGACTCGGCTT-3
***djr-1.1* external forward**	5-TCCGAAGTGCATACAAGGAG -3
***djr-1.1* external reverse**	5-GTTTCAGCCGAGAATACCGA-3
***djr-1.1* internal deletion**	5-TATGCCGGATTAGATGGAGC-3
***djr-1.2* external forward**	5-AGCAGTTCCAGGTCCTTTAG-3
***djr-1.2* external reverse**	5-GTTGAAGTCGGTCGTTGCAT-3
***djr-1.2* internal deletion**	5-ACTTGTAAACCTCCACGGAC-3
***Gene X* external forward**	5-AAAGGGGACTCTGGATCTTAGG-3
***Gene X* external reverse**	5-AGGAAGGCAGCGAGTTTGTT-3
***Gene X* internal deletion**	5-ACCTTGAGACCAAACAGACACA-3

Lifespan Assay:

Lifespan assays were performed at 20˚C in Thermo Scientific Precision incubators. The worms were synchronized by sodium hydrochlorite solution. L1 animals were then placed on NGM plates with 5X concentration *E. coli* OP50-1 (cultured in lysogeny broth overnight). Lifespan assays were performed utilizing 12.5 µl of 40 mM 5-fluoro-2-deoxyuridine (FUdR) at L4 to inhibit germline and progeny development. Animals were scored every 2 days on 60 mm NGM plates with regular OP50-1 and drug plates. 45 to 60 worms were utilized per experiment. Animal viability was assessed by prodding the worm gently and visually confirming movement. Animals were eliminated from the experiment if they had internal hatching or escaped the walls of the plate.

Touch Assay (Hyperesthesia):

Sensory response to eyelash was adapted from an assay previously described by Hobert et al. (51). The animals were touched, alternating between the anterior and the posterior with the eyelash, resulting in 30 times per animal. If the animal reversed direction after an anterior touch, the animal was scored as responding to touch, which was then reset with a posterior touch. Touch index (TI) was generated by the amount of times an animal responded to the touch stimulus over the number of times they did not feel the stimulus.

Neurodegeneration Assay:

A neurodegenerative damage assay was conducted on both pan-neuronal and dopaminergic GFP reporter strains under different conditions and different stages of adulthood. Animals were paralyzed using 10 mM levamisole and mounted on a 2% agarose pad. The number of both pan-neuronal and dopaminergic neurons were examined under an upright stereofluorescent compound microscope (Olympus, Hamburg, Germany). Images were collected at 20X and 60X and assessed for neuronal damage through ImageJ software. Neuronal degeneration was assessed and quantified with a *dat-1* promoter-induced GFP label on the four cephalic sensilla (CEP) dendrites from nerve ring to the tip of the nose. Animals were scored as positive if the worms exhibited any dendrite loss, axonal blebbing (broken neurites), or axonal branching/outgrowth. Neuronal degeneration was assessed similarly to the dopaminergic neurons in pan-neuronal background. Damage was quantified as the percentage of worms having neuronal defects such as thinning, outgrowth, blebbing, or complete neuronal loss.

Real Time PCR:

Genetic expression was performed by quantitative reverse transcriptase polymerase chain reactions. Animals were synchronized and grown until Day 1 (24 hours after L4 stage) at 20˚C in Thermo Scientific Precision incubators in 5X OP50-1 *E.coli* on a NGM agar plate. Samples were then collected by washing animals from the plate with M9 buffer solution and collected in 1.7 ml graduated microcentrifuge tubes (VWR International, Radnor, Pennsylvania). We removed the M9 buffer before utilizing Quick-RNA MiniPrep Kit (Zymo Research, Irvine, CA) to isolate the mRNA. Concentration of mRNA was determined using a nanodrop (ThermoFisher Scientific, Waltham, MA). Using the concentration determined by the nanodrop, we calculated for 1 µg of RNA to be converted into cDNA so that all samples would be uniform. Next we used the iScript Reverse Transcription Supermix (Bio-Rad Laboratories, Hercules, California) to create cDNA. We did a 2x dilution of the cDNA by adding 20 µl of DEPC-water (VWR International, Radnor, Pennsylvania) to the 20 µl cDNA. We utilized SensiFast SYBR NO-ROX Kit (Bioline International, Toronto, Canada), cDNA, primer mix (1 µl DEPC-water and 2 µl primer (table 3)), and ran the reaction on a LightCycler 480 Instrument II (Roche Holding AG, Basel, Switzerland) to determine gene expression. Cycle threshold values were examined to see whether each gene was up or down regulated.

Table 4: qPCR Primer Sequences, baseline control is the gene that the rest of the genes are normalize to in the qPCR.

qPCR primers	Primer sequences
pmp-2 **forward (baseline control)**	**5-ATCTTTCAAAGCCAATCCTCGAC-3**
pmp-2 **reverse (baseline control)**	**5-GAGATAAGTCAGCCCAACTCC-3**
skn-1c **forward**	**5-GAGACGAGACGAAGAAGAGAC-3**
skn-1c **reverse**	**5-TGGATTGAGGTGTTGGACGA-3**
gst-4 **forward**	**5-CATGTTTGCAATGCTCAATGTG-3**
gst-4 **reverse**	**5-AAATGGAGTCGTTGGCTTCAG-3**
gcs-1 **forward**	**5-TTATTTCGAAACGAGCAACTGG-3**
gcs-1 **reverse**	**5-TGTCATGTTTGTATGCAGGATGAG-3**
glod-4 **forward**	**5-CTGAATATGAAAGTTCTTCGCCAC-3**
glod-4 **reverse**	**5-TCATCCTCTGAGCCATATCCA-3**
djr-1.1 **forward**	**5-AAGTAGAGTCTGGTGGGCTG-3**
djr-1.1 **reverse**	**5-GAGTACTTGTAGCCTCCTTTCTC-3**
djr-1.2 **forward**	**5-TACTGAACCTGTCAAATGTGCC-3**
djr-1.2 **reverse**	**5-CTCTGCCAGTTTGCTACATCC-3**
Gene X **forward**	**5-CAATGATGACAGGAGTAAGCCAG-3**
Gene X **reverse**	**5-AGCGAGTTTGTTGGGATGAC-3**

Nuclear localization expression assay:

A genetic expression assay was conducted using a translational reporter tagged with GFP. *Gene X* was crossed into a translational reporter that expressed GFP tagged skn-*1, gst-4,* or *gcs-1*. Crossed strains were then synchronized and grown until Day 1 at 25˚C in Thermo Scientific Precision incubators in 5X OP50-1 *E.coli* on NGM agar plates. At day 1, animals were transferred onto basal, MGO, and Arsenite NGM plates for 4 hours. Animals were then staged and paralyzed using 10 mM levamisole and mounted on a 2% agarose pad. Samples were examined under the previously mentioned stereofluorescent compound microscope. Images were collected at 20X and quantified for

nuclear localization using ImageJ software. Animals were quantified by the amount of localization foci seen within the animal. The phenotype for each animal was qualified as low if the number of foci was 5 or less, medium if the number of foci between 6 and 10, and high if the number of foci that 11 or more.

Statistical Analysis:

Statistical analyses of lifespan and touch data were performed utilizing GraphPad Prism 6 (GraphPad Software, Inc., La Jolla, CA). Survival curves were plotted using the Kaplan-Meier method. All pairwise quantifications were conducted using two- tailed student t-tests. Significance was determined by p value as follows: * (<0.5), ** (<0.01), *** (<0.001).

Results:

Recapitulating diabetic complication phenotypes in glyoxalase (*djr-1.1 and djr-1.2)* knockout mutants in *C. elegans.*

To recapitulate diabetic complications within the *C. elegans* model, we used *glod-4* (ortholog of human *GLO1*) mutants, to examine the effects that the impairment of the glyoxalase system can have on diabetics. Previously, our lab utilized the *glod-4* model and showed that when the glyoxalase gene was knocked out, a decreased lifespan and an exacerbation of diabetic complications were exhibited (26). These phenotypes are important because there are phenotypic effects that are shown in patients with diabetes. In our modeling of the *glod-4* mutant, the worm exhibited a similar reduced lifespan compared to wildtype, as was previously shown (Figure 6A,(26)).

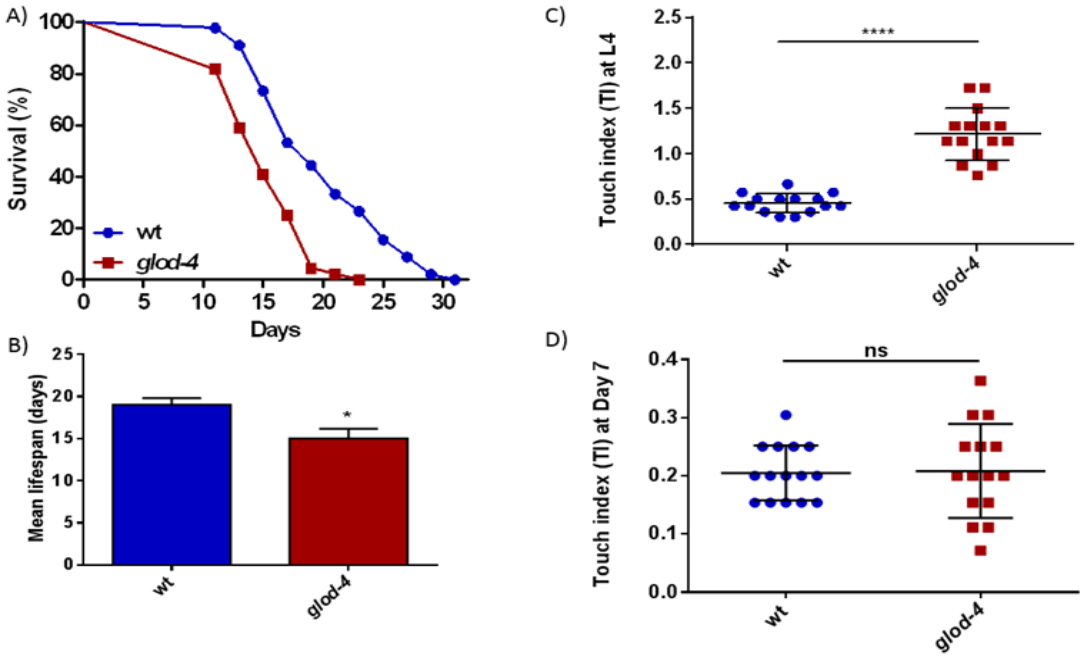

Figure 6: ***glod-4* KO leads to diabetic complications** Error bar depict standard deviation between worms. A) Lifespan curve, Wildtype (blue) and *glod-4* mutant (red) N = 45. B) Quantification of mean lifespan. C) Hyperesthesia assay at L4 stage, N=15 D) Hyperesthesia assay at day 7, N=15. All pairwise quantifications were conducted using two- tailed student t-tests. Significance was determined by p value as follows: * <0.5, **** <0.0001, and ns: no significant difference.

To further examine and understand the glyoxalase system role in the effects on the quality of life in patients we examined secondary complications, hyperesthesia and neuronal degeneration.

Hyperesthesia is a pathological phenotype that causes patients to be hypersensitive to touch. Previously, it was shown that when the glyoxalase gene *glod-4* was inhibited, mutants had increased hyperesthesia and showed the most sensitivity at early developmental Larval stage (L4) (Figure 6B). As the *C. elegans* aged, we saw

damage accumulate, as the touch sensitivity of the day 7 mutants started to exhibit similar to wildtype as the neurons were slowly degenerating (Figure 6C).

To examine potential damage that could lead to age-dependent development of pathological phenotypes, we quantified neuronal integrity within pan-neuronal (OH438 *unc-4*(*e120*) II; *otIs117* IV. (*unc-33*p::GFP + *unc-4*(+))) and dopaminergic neuronal reporter backgrounds. We wanted to evaluate why the *C. elegans* are hyperesthetic early in life when the glyoxalase was inhibited but lose the phenotype later in life. As *glod-4* was inhibited, the neuronal degradation began as minor damage, such as neuronal thinning, and culminated into neuronal cell loss (Figure 7Ai and Bi). This further validated that the glod-*4* protects against α-dicarbonyl induced diabetic complications. While diabetes is prevalent when glyoxalases are knocked out, scientists have identified that in cases of long term diabetes the predisposition to neurodegenerative diseases like PD is greatly elevated. The increased risk of PD led us to further examine if in the dopaminergic neurons expression of α-synuclein would lead to exacerbation of neuronal degeneration pathological phenotypes within the *glod-4* mutant.

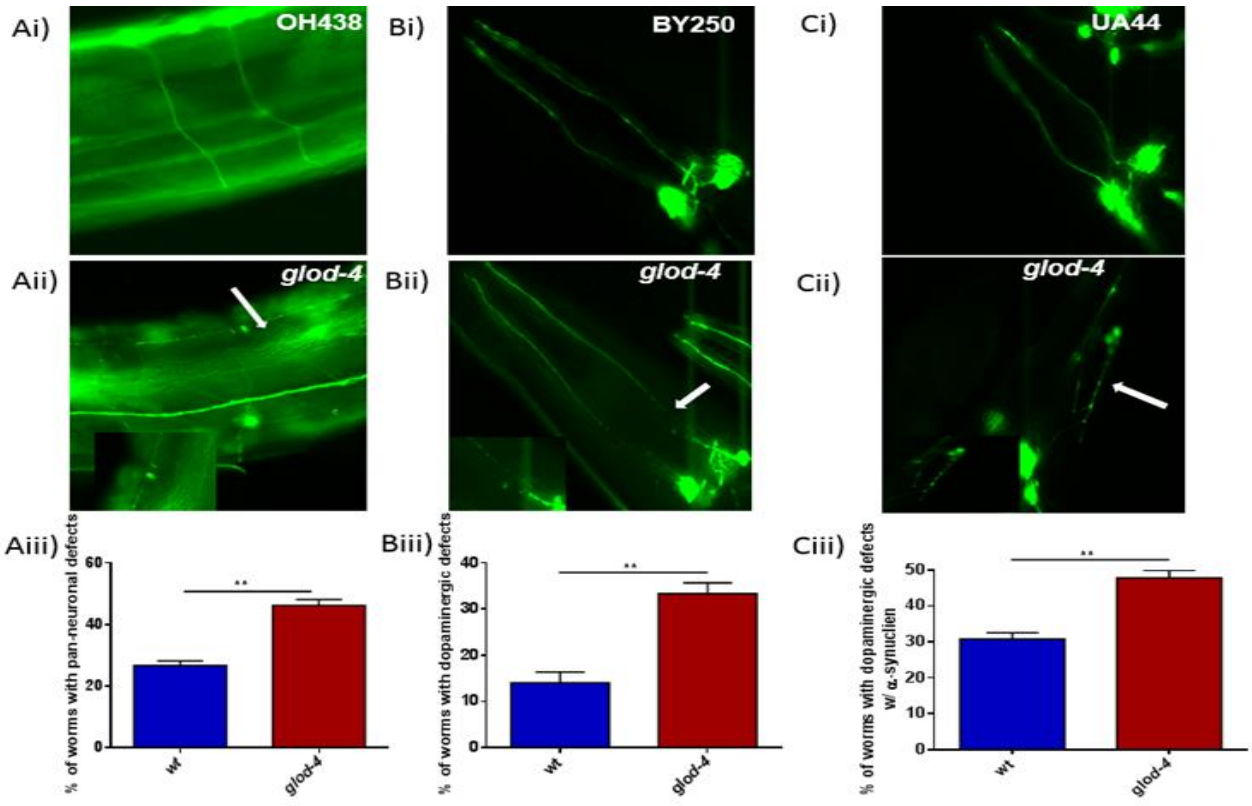

Figure 7: **Neurodegeneration utilizing the wildtype and *glod-4 mutant.*** Three independent GFP reporters were used and data was collected at Day 7 at 60X magnification. Ai) OH438 Pan-neuronal image of wildtype. All error bars depict standard deviation between worms. Aii) Pan-neuronal image of *glod-4* mutant. Neuronal breaks are identify by white arrow. Aiii) Quantification of neuronal damages of *glod-4* mutant's pan-neuronal neuron, N= 25. Bi) BY250 Dopaminergic neuronal images of wildtype. Bii) Dopaminergic neuronal images of *glod-4* mutant. Neuronal breaks are identify by white arrow. Biii) Quantification of neuronal damages of *glod-4* mutant's dopaminergic neuron (BY250), N= 25. Ci) UA44 Dopaminergic neuronal images with α-synuclein expression of wildtype. Cii) Dopaminergic neuronal images with α-synuclein expression of *glod-4* mutant. Neuronal branching are identify by white arrow. Ciii) Quantification of neuronal damages of *glod-4* mutant's dopaminergic neurons with α-synuclein expression (UA44), N= 25. All pairwise quantifications were conducted using two- tailed student t-tests. Significance was determined by p value as follows: * <0.5 and ** <0.01.

We found that in the PD model with the *glod-4* mutation, there was an exacerbation of neuronal damage. This demonstrates that diabetic complications were present and that there was further damage with the accumulation of α-synuclein expression compared to

the dopaminergic wildtype (Figure 7Aii-iii and Bii-iii). The elevation in neuronal damage with the dopaminergic neurons within the *glod-4* mutation led us to evaluate if glyoxalases plays a role in the association between diabetes and PD.

Elevated risk of PD led us to investigate the human *DJ1* gene, which is known to be associated with PD as it was discovered to be a novel glyoxalase gene (37). Mutations to *djr-1.1* and *djr-1.2*, the worm orthologs for human *DJ1*, also caused a reduced lifespan similar to the *glod-4* mutant (Figure 8A and B).

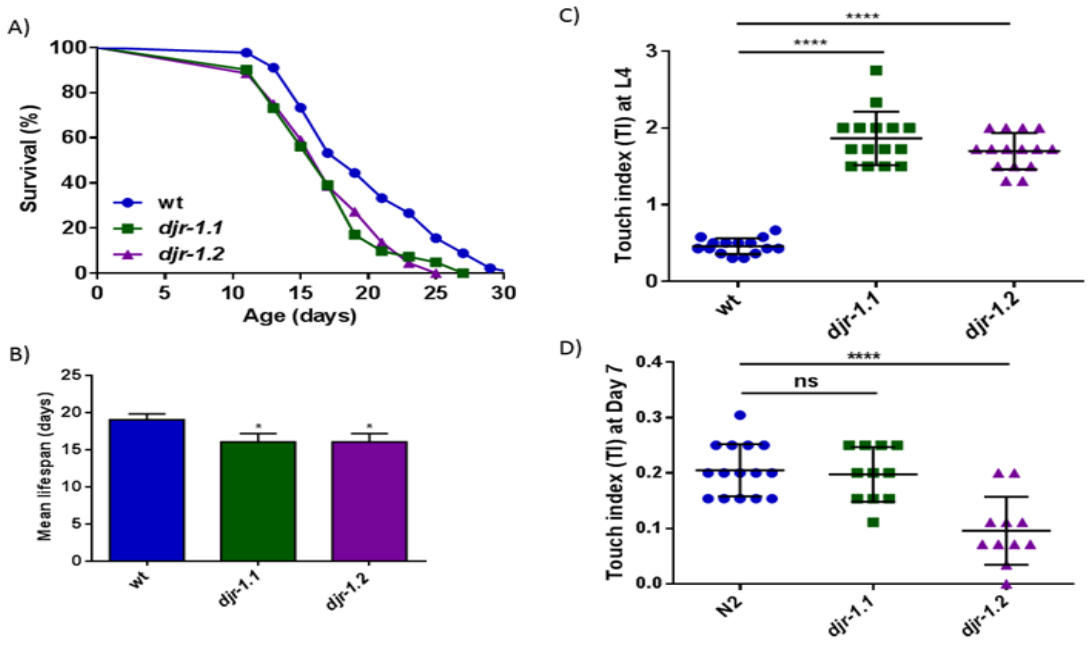

Figure 8: ***djr-1.1 and djr-1.2* KO leads to Parkinson's Disease phenotypes** Error bar depict standard deviation between worms. A) Lifespan curve (Top) wildtype (blue), *djr-1.1* mutant (green), and *djr-1.2* mutant (purple), N = 45. B) Quantification of mean lifespan. C) Hyperesthesia assay at L4 stage, N=15 D) Hyperesthesia assay at day 7, N=15 All pairwise quantifications were conducted using two- tailed student t-tests. Significance was determined by p value as follows: * <0.5, **** <0.0001, and ns: no significant difference.

With the reduction of lifespan similar to the diabetic model we further examined other diabetic complications phenotypes in these mutants. Scientists have seen a lower threshold to pain in PD patients, known as hyperalgesia (52). We discovered that the *djr1-1* and *djr-1.2* mutants demonstrated elevated hypersensitivity to touch at early developmental stages (Figure 8C). However, like the *glod-4* glyoxalase mutant as the worms were aged to day 7 there was an age-dependent loss of hyperesthesia (Figure 8D). Interestingly, we saw that depending on the tissue-specific expression pattern of djr-*1.1* and *djr-1.2* genes, there was an age-dependent effect in hyperesthesia at day 7. *djr-1.2,* which is mainly expressed in the neurons, exhibited a significant loss in touch sensitivity compare to wildtype, whereas *djr-1.1,* mainly expressed in the intestines, had no significant difference compared to the wildtype (Figure 8C).

To solidify the association between diabetic complications and PD, we looked at neuronal integrity which allowed us to better understand the hyperesthesia seen in these glyoxalase *djr-1.1* and *djr-1.2* mutants. Utilizing the pan-neuronal GFP strains, we saw that within these animals there was severe neuronal degradation phenotypes, such as blebbing, as they aged (Figure 9Ai and Bi).

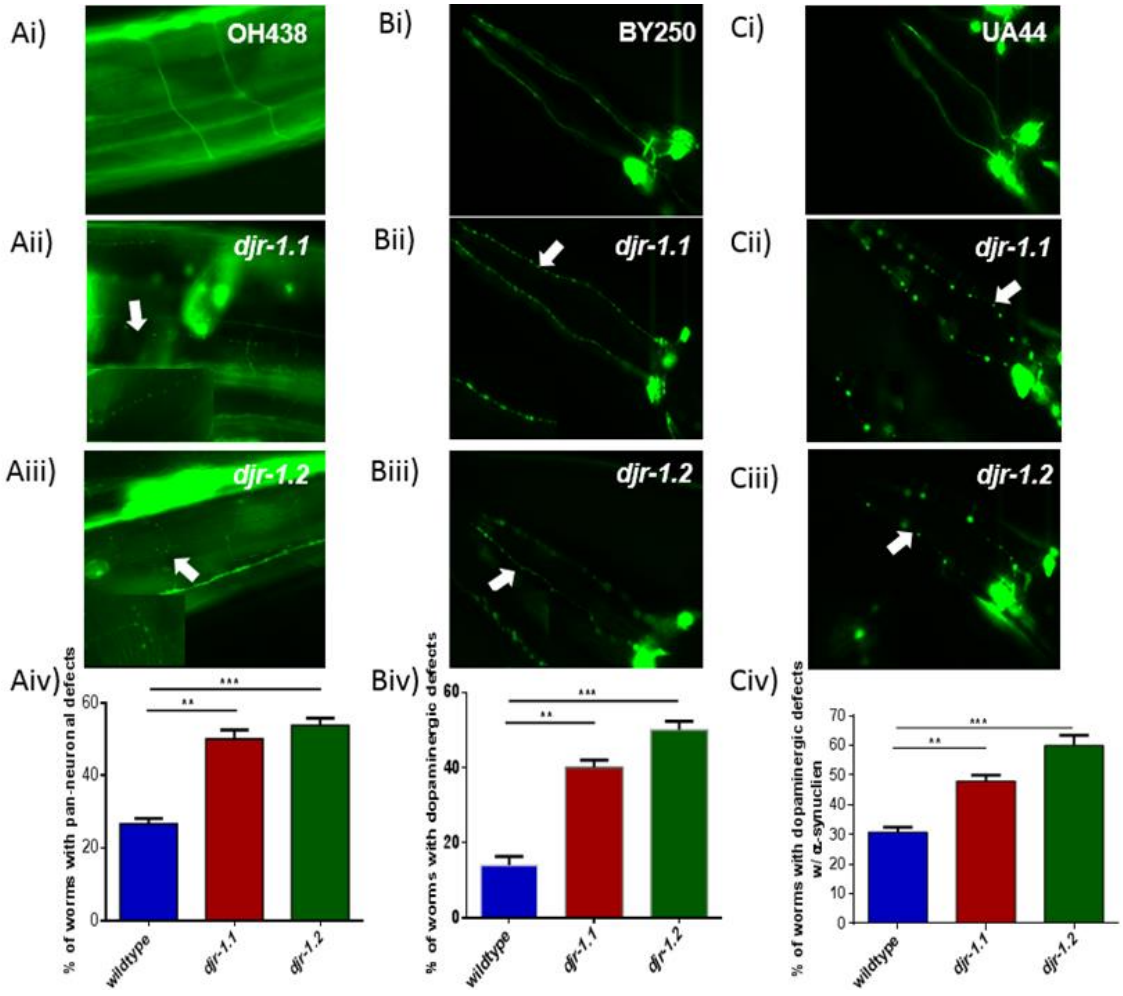

Figure 9 **Neurodegeneration utilizing the wildtype, *djr-1.1,* and *djr-1.2* mutants**. Three independent GFP reporters were used and data was collected at Day 7. Ai) OH438 Pan-neuronal image of wildtype. All error bar depict standard deviation between worms. All white arrow depict blebbing leading to neuronal loss. Aii) Pan-neuronal image of *djr-1.1* mutant. Aiii) Pan-neuronal image of *djr-1.2 mutant.* Aiv) Quantification of neuronal damages of *djr-1.1 and djr-1.2* mutants' pan-neuronal neuron, N= 25. Bi) BY250 Dopaminergic neuronal images of wildtype. Bii) Dopaminergic neuronal images of *djr-1.1 mutant*. Biii) Dopaminergic neuronal images of *djr-1.1* mutant. Biv) Quantification of neuronal damages of *djr-1.1 and djr-1.2* mutants' dopaminergic neuron (BY250), N= 25. Ci) UA44 Dopaminergic neuronal images with α-synuclein expression of wildtype. Cii) Dopaminergic neuronal images with α-synuclein expression of *djr-1.1* mutant. Ciii) Dopaminergic neuronal images with α-synuclein expression of *djr-1.2* mutant. Civ) Quantification of neuronal damages of *djr-1.1 and djr-1.2 mutants'* dopaminergic neurons with α-synuclein expression (UA44), N= 25. All pairwise quantifications were conducted using two- tailed student t-tests. Significance was determined by p value as follows: * <0.5 and ** <0.01.

We next examined dopaminergic neurons with a dopaminergic neuron reporter strain (BY250 *vtIs7*[*Pdat-1*::GFP] (53)) to examine if the djr-*1.1* and djr-1.2 mutants could further exacerbate the neuronal damage in an age-dependent manner within the dopaminergic neurons. In the BY250 wildtype strain, as the worms aged from early adult stage to day 7 there was a slow, minor degeneration of neurons. However, when the *djr-1.1* and *djr-1.2* glyoxalase genes were inhibited within the BY250 strain, this disease model exhibited to severe phenotypic consequences such as blebbing and complete cell loss (Figure 9Aii and Bii), which is reminiscent of PD patients whose dopaminergic neurons are undergoing cell death. Another phenotype seen in human PD patients is aggregation of α-synuclein within the dopaminergic neurons that further contributes to neuronal damage. In order to evaluate the role of α-synuclein, we utilized a dopaminergic neuronal strain that expresses α-synuclein (UA44 *baIn11*(*Pdat-1*:: α-syn, *Pdat-1*::GFP) (54)) with the *djr-1.1* and *djr-1.2* mutants. When examined, the *djr-1.1* and *djr-1.2* knockouts exhibited a further acceleration of neuronal damage within the animal's dopaminergic neurons, in association with the expression of α-synuclein, compared to the wildtype and BY250 control. (Figure 9Aiii and Biii).

Diabetic Complication Gene *X* leads to lifespan extension, alleviation of neurodegeneration, and reduces hyperesthesia in the glyoxalase mutants.

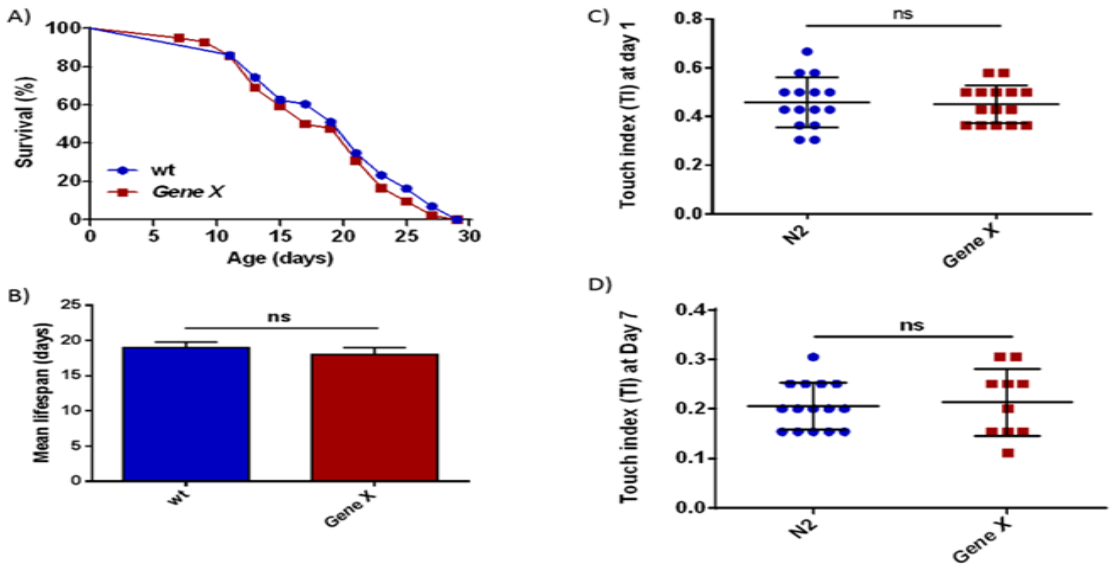

Figure 10: ***Gene X KO* protects against diabetic complications.** Error bars depict standard deviation between worms. A) Lifespan curve (Top) wildtype (blue) and *Gene X* mutant (red) N = 45. B) Quantification of mean lifespan. C) Hyperesthesia assay at L4 stage, N=15 D) Hyperesthesia assay at day 7, N=15. All pairwise quantifications were conducted using two- tailed student t-tests. Significance was determined by p value as follows: ns: no significant difference.

Recently, a GWAS study identified novel human SNPs associated with diabetic complication of cardiomyopathy and nephropathy [11]. Our lab performed a Blast analysis to identify the worm ortholog of the human genes that contained these SNPS. 20 worm genes were successfully identified. Initially, we sought to establish whether mutations in these genes displayed phenotypic similarities to the glyoxalase mutants in worms. A preliminary lifespan assay was conducted on wildtype and *glod-4* glyoxalase mutant worms treated with RNAi for the 20 candidate genes. Through this screen, we

found that Gene *X* RNAi rescued the lifespan in the *glod-4* mutant's, whereas RNAi of 3 other genes exacerbated the pathological phenotypes (Table 1). The remaining 16 genes, did not induce significant changes (data not shown) in pathological effects. Next, we wanted to examine if newly acquired *Gene X* null *C. elegans* mutants from the Bargmann Lab at Rockefeller University, New York (47) could exhibit similar phenotypes to the *Gene X* RNAi worm. Utilizing the *Gene X* null mutant, we discovered that it exhibited a lifespan that was similar to the wildtype (Figure 10A and B). To further confirm that *Gene X* had a potential effect on diabetes and PD, we modeled the hyperesthesia and neurodegeneration within the *Gene X* mutant. *Gene X* null mutants exhibited similar results to wildtype for hyperesthesia, both at early L4 stage and day 7 (Figure 10C and D). When examining the neuronal integrity of both pan-neuronal and dopaminergic neurons, we saw that both reporters exhibited no significant damages, similar to wildtype (Figure 11Ai-iii and Bi-iii). Next, we examining α-synuclein expression in the *Gene X* mutant and saw that, compared to the wildtype, there was also no significant damage (Figure 11Ci-iii). The data shows that mutations in *Gene X* are not significantly different than wildtype worms for the characteristics such as lifespan, hyperesthesia, and neurodegeneration.

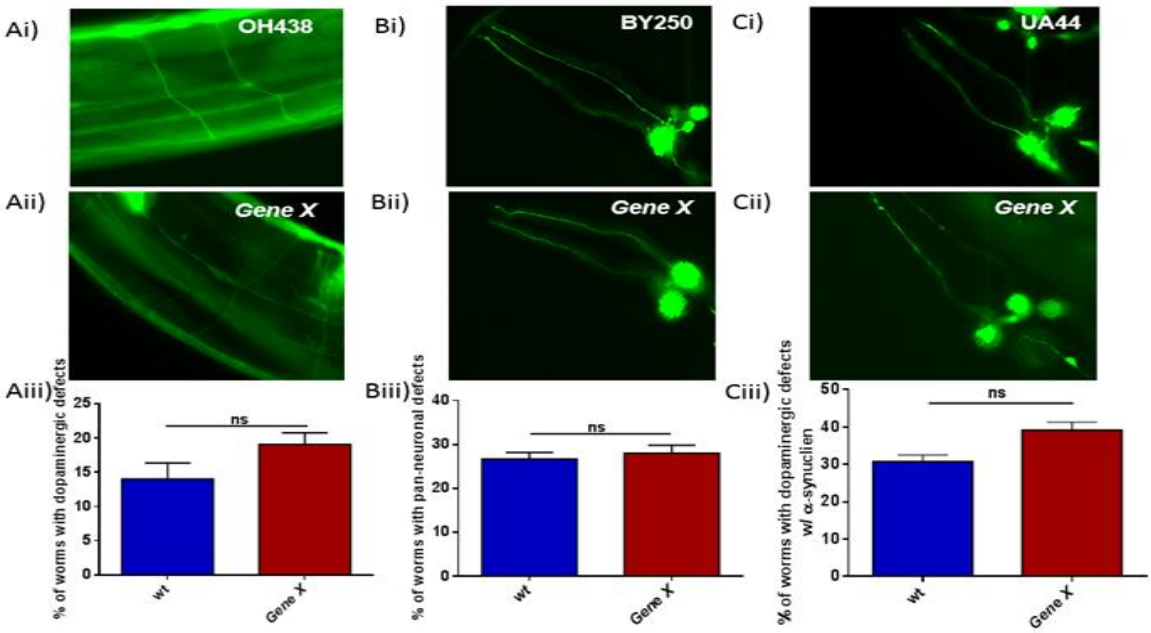

Figure 11: **Neurodegeneration utilizing the wildtype and *Gene X* mutant.** Three independent GFP reporters were used and data was collected at Day 7 at 60X magnification. All error bar depict standard deviation between worms. Ai) OH438 Pan-neuronal image of *wildtype.* Aii) Pan-neuronal image of *Gene X* mutant. Aiii) quantification of neuronal damages of *Gene X* mutant's pan-neuronal neuron, N= 25. Bi) BY250 Dopaminergic neuronal images of wildtype. Bii) Dopaminergic neuronal images of *Gene X* mutant. Biii) quantification of neuronal damages of *G*ene X mutant's dopaminergic neuron (BY250), N= 25. Ci) UA44 Dopaminergic neuronal images with α-synuclein expression of wildtype. Cii) Dopaminergic neuronal images with α-synuclein expression of *Gene X* mutant. Ciii) quantification of neuronal damages of *Gene X* mutant's dopaminergic neurons with α-synuclein expression (UA44), N= 25. All pairwise quantifications were conducted using two- tailed student t-tests. Significance was determined by p value. ns: not significant

In order to better understand the role of inhibiting *Gene X* in diabetic complications, we utilized the glyoxalase mutant *glod-4* model to examine the same phenotypes. As *Gene X* was knocked out simultaneously with glod-*4* mutation, we saw an alleviation of their reduced lifespan, which was reminiscent of the RNAi (Figure 12A and B). Next, we looked at other diabetic complication-specific phenotypes, such as

hyperesthesia, to see if the alleviation effects would be recapitulated. The double knockout exhibited an alleviation of hyperesthesia approaching levels similar to wildtype at early stages (Figure 12C). The older day 7 double knockout mutants did not have a significant alleviation of the hyperesthesia phenotypes (Figure 12D).

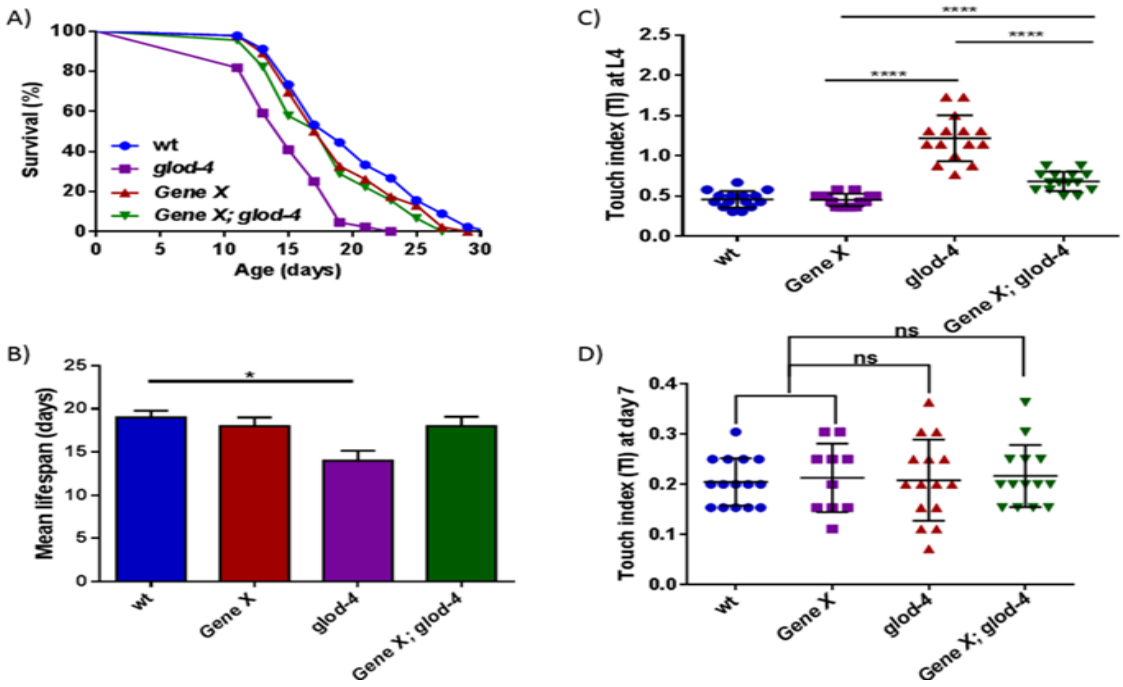

Figure 12: ***Gene X KO* protects against diabetic complications in *glod-4* mutant.** Error bar depict standard deviation between worms. A) Lifespan curve (Top) wildtype (blue), *Gene X* mutant (red), *glod-4* mutant (purple), and *Gene X; glod-4* mutant (green), N = 45. B) Quantification of mean lifespan. C) Hyperesthesia assay at L4 stage, N=15 D) Hyperesthesia assay at day 7, N=15. All pairwise quantifications were conducted using two- tailed student t-tests. Significance was determined by p value as follows: * <0.5, **** <0.0001, and ns: no significant difference.

To determine if *Gene X* had a role in neuronal protection, we examined the neural integrity within these mutants. The double mutant exhibited an improvement in pan-neuronal integrity compared to the single *glod-4* mutation (Figure 13Ai-iii). Furthermore, we utilized the dopaminergic neuronal reporter BY250 to examine the associations that diabetes plays to Parkinson's Disease. In the dopaminergic control, we saw similar effects to the pan-neuronal reporter. There was an alleviation effect of the neuronal damage compared to the single mutant (Figure 13Bi-iii).

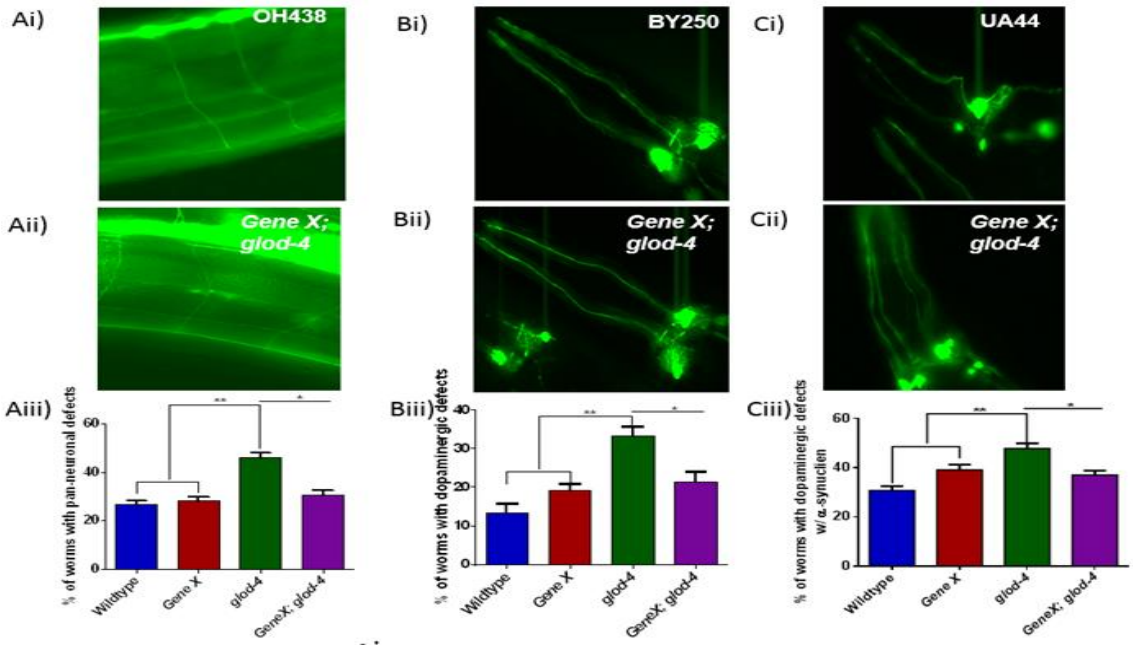

Figure 13: **Neurodegeneration utilizing the wildtype and *Gene X; glod-4* mutant.** Three independent GFP reporters were used and data was collected at Day 7 at 60X magnification. All error bar depict standard deviation between worms. Ai) OH438 Pan-neuronal image of *wildtype.* Aii) Pan-neuronal image of *Gene X; glod-4* mutant. Aiii) quantification of neuronal damage of *Gene X; glod-4* mutant's pan-neuronal neuron, N= 25. Bi) BY250 Dopaminergic neuronal images of wildtype. Bii) Dopaminergic neuronal images of *Gene X; glod-4* mutant. Biii) quantification of neuronal damage of *G*ene X; *glod-4* mutant's dopaminergic neuron (BY250), N= 25. Ci) UA44 Dopaminergic neuronal images with α-synuclein expression of wildtype. Cii) Dopaminergic neuronal images with α-synuclein expression of *Gene X; glod-4* mutant. Ciii) quantification of neuronal damage of *Gene X; glod-4* mutant's dopaminergic neurons with α-synuclein expression (UA44), N= 25. All pairwise quantifications were conducted using two- tailed student t-tests. Significance was determined by p value as follows: * <0.5 and ** <0.01

Subsequently, we concluded that when *Gene X* is mutated it induces a protective effect against diabetic complications. To further connect PD and diabetes, we examined the double knockout in the α-synuclein expression using the dopaminergic reporter and examined the effect on neuronal damage. When *Gene X* was mutated, there was an alleviation of neuronal damage from the accumulation seen in the *glod-4* mutant,

bringing levels back to those seen in the wildtype (Figure 13Ci-iii). With the alleviation of pathological phenotypes seen in these double mutants, we wanted to examine whether *Gene X* mutation can also play a role specifically in the Parkinson disease related glyoxalase *djr-1.1* and *djr-1.2* genes.

When examining double mutants in *Gene X* and either *djr-1.1* or *djr-1.2,* we found that the diabetic complications were alleviated. Similar to the double mutant with *glod-4,* the reduced lifespan of *djr-1.1 and djr-1.2* was extended when *Gene X* was knocked out (Figure S1A and 14A). Next, we found that the double mutant of *Gene X* with *djr-1.1* or *djr-1.2* exhibited touch sensitivity similar to the wildtype at younger stages, demonstrating a rescue of the single *djr-1.1* and *djr-1.2* mutations (Figure S1B and 14B). Interestingly, as we further aged the mutant strains depending on tissue specific expression there was a different effect in the alleviation of pathological phenotypes. Within worms with *djr-1.1* intestinal expression, there was not a significant alleviation of touch sensitivity compared to wildtype (Figure S1C), while within the *djr-1.2* neuronal expression there was a slight alleviation touch sensitivity compared to the single *djr-1.2* mutant at day 7 (Figure 14C).

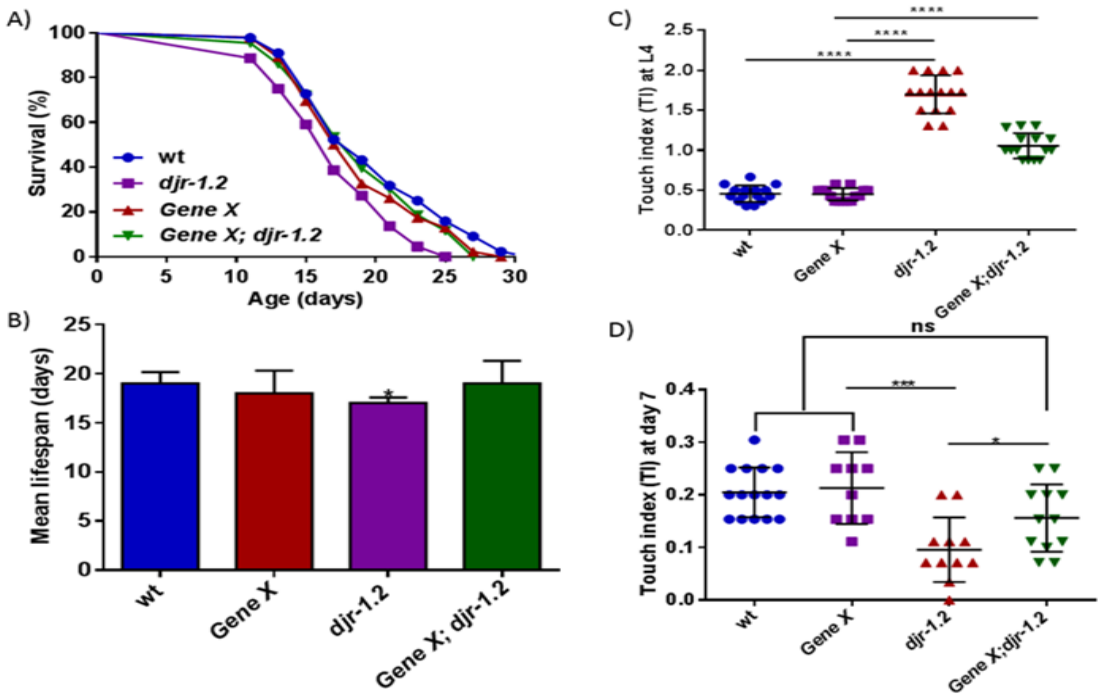

Figure 14: ***Gene X KO* protects against diabetic complications in *djr-1.2* mutant.** Error bar depict standard deviation between worms. A) Lifespan curve (Top) wildtype (blue), *Gene X* mutant (red), *djr-1.2* mutant (purple), and *Gene X; djr-1.2* mutant (green), N = 45. B) Quantification of mean lifespan. C) Hyperesthesia assay at L4 stage, N=15. D) Hyperesthesia assay at day 7, N=15 All pairwise quantifications were conducted using two- tailed student t-tests. Significance was determined by p value as follows: * <0.5, **** <0.0001, and ns: no significant difference.

Next, we examined if the Gene *X* mutation could play a role in alleviating these neurological phenotypes in *djr-1.1* and *djr-1.2* mutants. In the pan-neuronal strain, *Gene X* mutants demonstrated a rescue of neuronal integrity within the *djr-1.1* and *djr-1.2* double mutants by alleviating neuronal damage phenotypes (Figure S2Ai, S2Bi, 15Ai, and 15Bi). As the pan-neuronal reporter showed an alleviation effect, we further

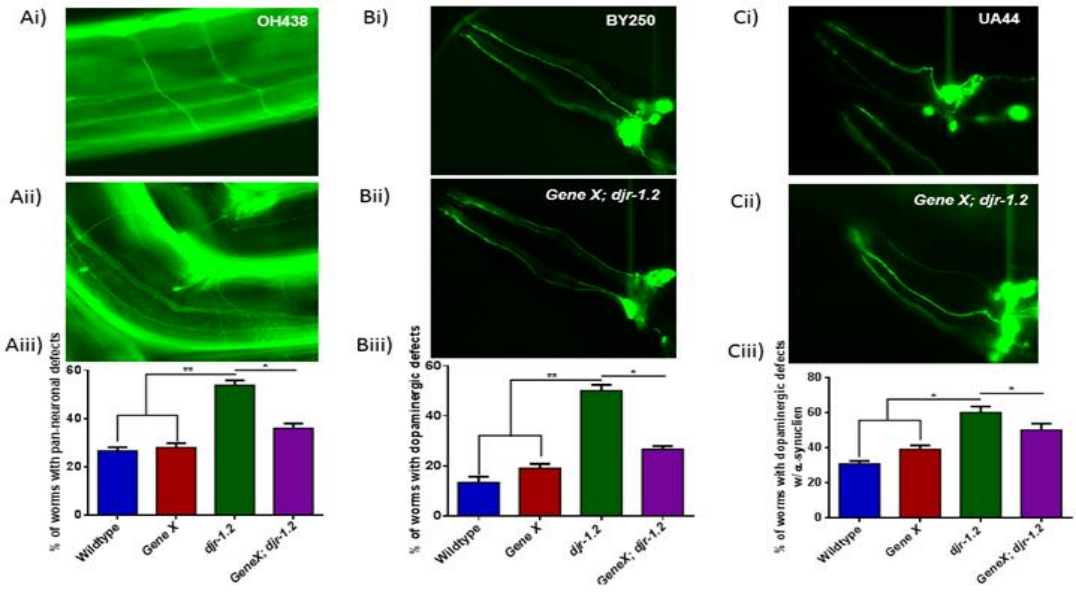

Figure 15: **Neurodegeneration utilizing the wildtype and *Gene X; djr-1.2* mutant.** Three independent GFP reporters were used and data was collected at Day 7 at 60X magnification. All error bar depict standard deviation between worms. Ai) OH438 Pan-neuronal image of *wildtype.* Aii) Pan-neuronal image of *Gene X; djr-1.2* mutant. Aiii) quantification of neuronal damages of *Gene X; djr-1.2 mutant's* pan-neuronal neuron, N= 25. Bi) BY250 Dopaminergic neuronal images of wildtype. Bii) Dopaminergic neuronal images of *Gene X; djr-1.2 mutant*. Biii) quantification of neuronal damages of *G*ene X; *djr-1.2* mutant's dopaminergic neuron (BY250), N= 25. Ci) UA44 Dopaminergic neuronal images with α-synuclein expression of wildtype. Cii) Dopaminergic neuronal images with α-synuclein expression of *Gene X; djr-1.2 mutant*. Ciii) quantification of neuronal damages of *Gene X; djr-1.2 mutant's* dopaminergic neurons with α-synuclein expression (UA44), N= 25. All pairwise quantifications were conducted using two- tailed student t-tests. Significance was determined by p value as follows: * <0.5 and ** <0.01

examined the effect in the PD-specific dopaminergic reporter. We utilized the dopaminergic reporter to help us evaluate the specific pathologies associated with Parkinson's Disease exhibited in with the *djr-1.1* or *djr-1.2* knockouts. By crossing the *Gene X* mutant strain to the *djr-1.1* and *djr-1.2* mutants, we were able to examine potential effects that could occur similarly to the pan-neuronal expression. When we examined the dopaminergic neuron reporter BY250, we noticed that the *djr-1.1* and *djr-1.2* mutants produced neuronal blebbing and cell loss, which was alleviated with *Gene X* knockout (Figure S2Aii, S2Bii, 12Aii, and 12Bii). To better understand if Gene *X* knockout can have a role in alleviating the damage incurred by most PD mutations, we specifically examined *djr-1.1* and *djr-1.2* mutants with the α-synuclein expression dopaminergic neuronal reporter [28]. This led to further exacerbation of the severe neuronal phenotype, however with *Gene X* inhibition in these glyoxalase mutants there was a protective effect (Figure S2Aiii, S2Biii, 15Aiii, and 15Aiii). After establishing that *Gene X* knockout can be protective against the glyoxalases mutants, we wanted to determine if accumulation of the toxic α-dcs, such as MGO, could further exacerbate pathological phenotypes in single mutants. Furthermore, we also wanted to evaluate if *Gene X* mutations could protect against oxidative stress induced by the addition of exogenous MGO.

Gene *X* protect against Oxidative Stress produce by exogenous Methylglyoxal

Addition of exogenous methylglyoxal (MGO), one of the α-dicarbonyl compounds, increases oxidative stress in *C. elegans* and leads to diabetic complication [8] and neurodegenerative diseases in the glyoxalase *glod-4* mutant (26). In our examination of exogenous addition of MGO, we saw that for the single *Gene X* mutation there was no significant effect on lifespan compared to wildtype (Figure 16A).

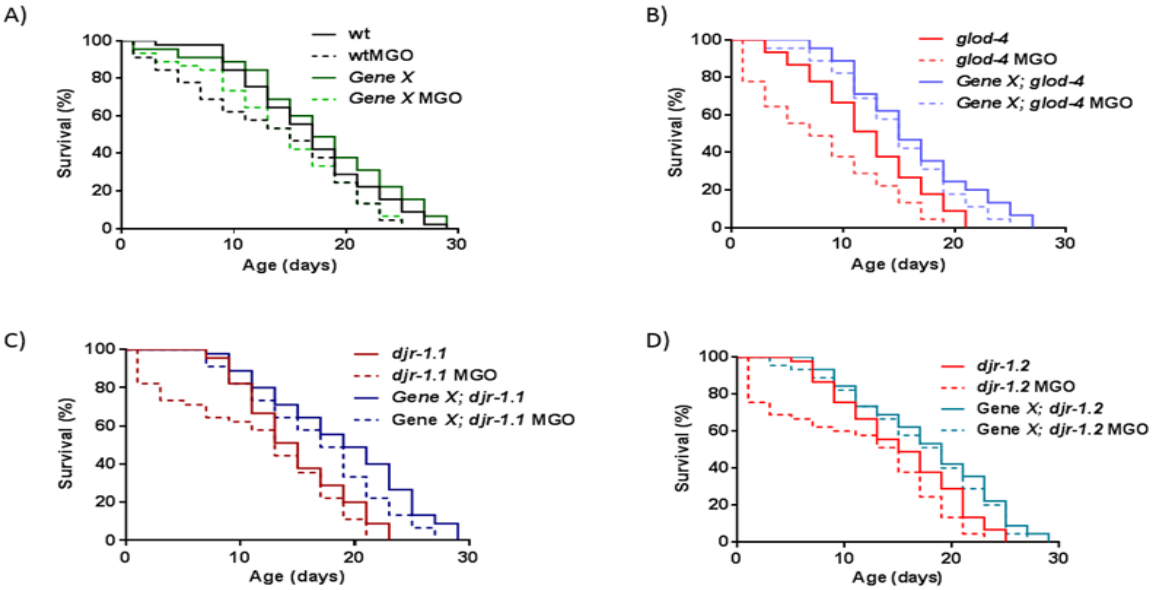

Figure 16: **Oxidative stress with addition of exogenous MGO on glyoxalase mutants, *Gene X mutant,* and *Gene X;* glyoxalase mutants.** Exogenous 7mM MGO addition with N= 45. A) Stress curves wildtype (black solid), wildtype +MGO (black dash), *Gene X* (green solid), and *Gene X* +MGO (green dash).B) Stress curves *gold-4* (red solid), *glod-4* +MGO (red dash), *Gene X; glod-4* (blue solid), and *Gene X; glod-4* +MGO (blue dash). C) Stress curves *djr-1.1* (red solid), *djr-1.1* +MGO (red dash), *Gene X; djr-1.1* (blue solid), and *Gene X; djr-1.1* +MGO (blue dash). D) Stress curves *djr-1.2* (red solid), *djr-1.2* +MGO (red dash), *Gene X; djr-1.2* (blue solid), and *Gene X; djr-1.2* +MGO (blue dash).

However, we saw that exogenous MGO stress reduced lifespan of the single *glod-4* mutant further (Figure 16B). Conversely, we found that in the double *Gene X; glod-4* mutant, the exogenous MGO addition did not have a significant reduction in lifespan (Figure 16B). Then, we examined α-dicarbonyl stress and its association with PD by adding exogenous MGO to the *djr-1.1* and *djr-1.2* mutants. At the beginning of the *djr-1.1* and *djr-1.2* lifespan, the worms experienced significant damage from the oxidative stress and exhibited a significant reduction of lifespan (Figure 16C and D).

Next, we examined the neurodegeneration phenotype to evaluate if adding exogenous MGO would have a phenotypic effect on the *Gene X; glyoxalase* mutants. As with the *Gene X* mutation on its own, we observed no significant effect similar on lifespan (Figure S3A). When the *Gene X* mutation was added to the diabetic *glod-4* mutant model with exogenous MGO added, we saw that there was a significant alleviation effect from the *glod-4* mutation alone, however there was no significance between the double mutants with oxidative stress compared to basal conditions (Figure S3B). Through the addition of exogenous addition of MGO to the *djr-1.1* and *djr-1.2* mutants, similarly to the *Gene X;glod-4* double mutant we observed an alleviation of neuronal damage that was not significantly different from the basal condition (Figure S3C and D).

A)

Rank	Motif	Best Match/Details
1		skn-1/MA0547.1/Jaspar(0.589) More Information | Similar Motifs Found
2		che-1/MA0260.1/Jaspar(0.666) More Information | Similar Motifs Found
3		POL004.1_CCAAT-box/Jaspar(0.669) More Information | Similar Motifs Found

B)

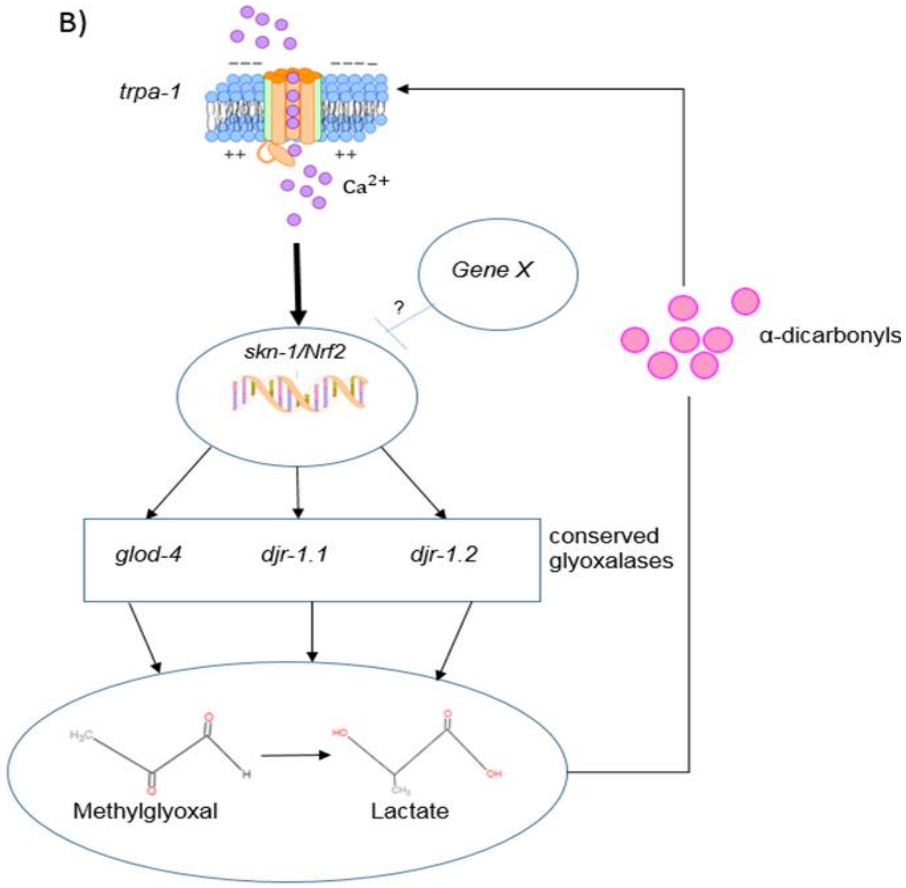

Figure 17: **Hypothesis of potential pathway for *Gene X* and *skn-1* interaction.** A) Motif enrichment analysis utilizing Homer algorithm (Courtesy: Brian Hodge) reveals skn-1 to be the best match hit for hmbx-1‘s DNA binding motifs. *B) trpa-1/skn-1* pathway with hypothesized *Gene X* interaction to *skn-1 as a transcriptional repressor.*

Determination of Gene *X* function through gene expression and its connection to the *trpa-1/skn-1* pathway.

We next investigated what potential genetic targets *Gene X* utilizes to detoxify excess α-dicarbonyls. Utilizing a worm *Gene X* ChiP-seq data set that is available online from Encyclopedia of DNA Elements (ENCODE) database (55), we performed an *in silico* motif enrichment analysis using the Homer algorithm. A top potential target for *Gene X* was identified to be a skn-*1* binding site (Figure 17A). We hypothesized that *Gene X* could be influencing the *trpa-1/skn-1* pathway, which our lab previously studied (26) as a repressor for *skn-1* (Figure 17B). This corresponds to previous work that has shown that *Gene X* is a transcriptional repressor for multiple pathways ((47), (48), and (49)).

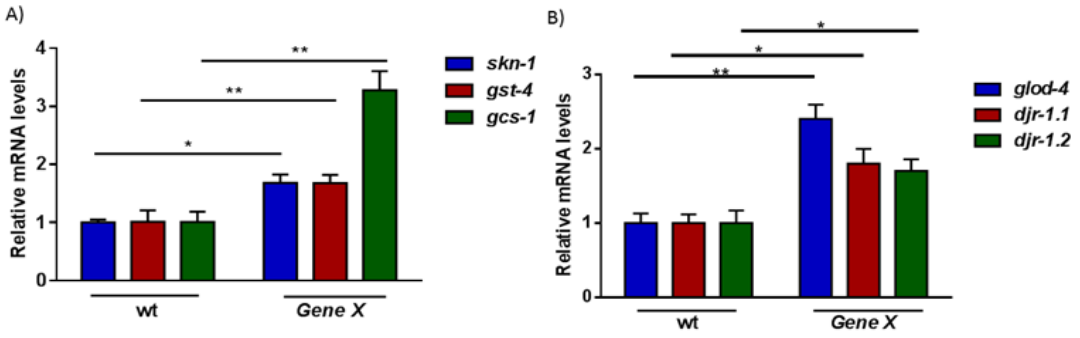

Figure 18: **Gene *X* KO at basal conditions upregulates *skn-1* and its downstream targets.** All data normalized to wildtype and expression levels of *pmp-2* gene. All error bar depict standard deviation in samples. A) Relative expression of *skn-1*, *gst-4*, and *gcs-1 in* wildtype compare to *Gene X* KO in basal conditions. B) Relative expression of *glod-4*, *djr-1.1*, and *djr-1.2 in* wildtype compare to *Gene X* KO in basal conditions. All pairwise quantifications were conducted using two- tailed student t-tests. Significance was determined by p value as follows: * <0.5 and ** <0.01.

In order to confirm this potential interaction, we examined the expression pattern of *skn-1* and its downstream targets in the *Gene X* mutant background. We also over

expressed *Gene X using* an overexpressor line, which has two copies of *Gene X*, one tagged with GFP. We examined the expression of *skn-1* and its downstream targets *gst-4* and *gcs-1*. We found that *skn-1,* gcs-*1,* and *gst-4* all were significant upregulated in the *Gene X* mutant compared to the wild type (Figure 18A). We hypothesized that upregulation of *skn-1, gst-4,* and *gcs-1* in *Gene X* mutants could lead to further induction of the glyoxalase genes, resulting in further detoxification of the α-dcs. We then examined the glyoxalase genes to see if there were any expression changes when *Gene X* was inhibited. We examined the expression of *glod-4, djr-1.1,* and *djr-1.2,* and found there was a significant upregulation of the glyoxalase levels within the *Gene X* mutant compared to the wildtype (Figure 18B). Utilizing the *Gene X* overexpression we compared the differences in *skn-1, gst-4, gcs-1,* and glyoxalase expression to the expression levels of the *Gene X* knockout alone. *Gene X* overexpression was found to have a repressive effect on the expression of *skn-1, gst-4, gcs-1,* and glyoxalase targets, exhibiting expression levels similar to the wildtype (data not shown). When *Gene X* was downregulated, the clearance rate of toxic compounds was hindered, thus leading to accumulation of these compounds.

Toxic compounds continuously accumulate with *Gene X* downregulation and oxidative stress and related damage also accumulate throughout the body. As stress accumulates and free α-dicarbonyls travel in the vascular system, the *trpa-1* receptor then activates the glyoxalase detoxification pathway (26). To examine the induction of oxidative stress utilizing the *trpa-1/skn-1* pathway, we added exogenous MGO which leads to an induction in *skn-1* expression caused by the activation of *trpa-1*. In order to determine if MGO does work as an oxidative stressor, we utilized an Arsenite positive

control as it is known to acts as a s*kn-1* inducer in oxidative stress [23]. In the oxidative stress conditions, we compared the *Gene X* mutant and the wildtype to determine if there were any differences in genetic expression of *skn-1, gst-4,* and *gcs-1* compared to the basal conditions. Similar to basal conditions the MGO significantly upregulated the expression of *skn-1, gst-4, and gcs-1* genes in *Gene X* mutants compare to the wildtype (Figure 19A).

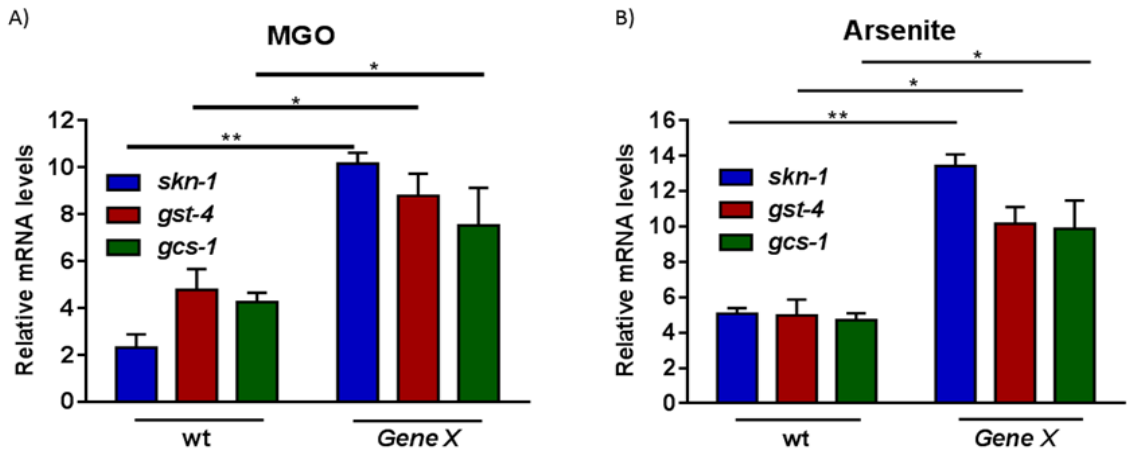

Figure 19: **Gene *X* KO at stress conditions further upregulates skn-*1* and its downstream targets.** All data normalized to wildtype and expression levels of *pmp-2* gene. All error bar depict standard deviation in samples. A) Relative expression of *skn-1, gst-4,* and *gcs-1* in wildtype compare to *Gene X* KO in treatment of MGO. B) Relative expression of *skn-1, gst-4,* and *gcs-1* in wildtype compare to *Gene X* KO in treatment of Arsenite. All pairwise quantifications were conducted using two- tailed student t-tests. Significance was determined by p value as follows: * <0.5 and ** <0.01.

As a positive control in the oxidative stress condition induced by Arsenite, we also determined that there was a significant upregulation of gene expression in the *Gene X* knockout compared to the wildtype (Figure 19B).

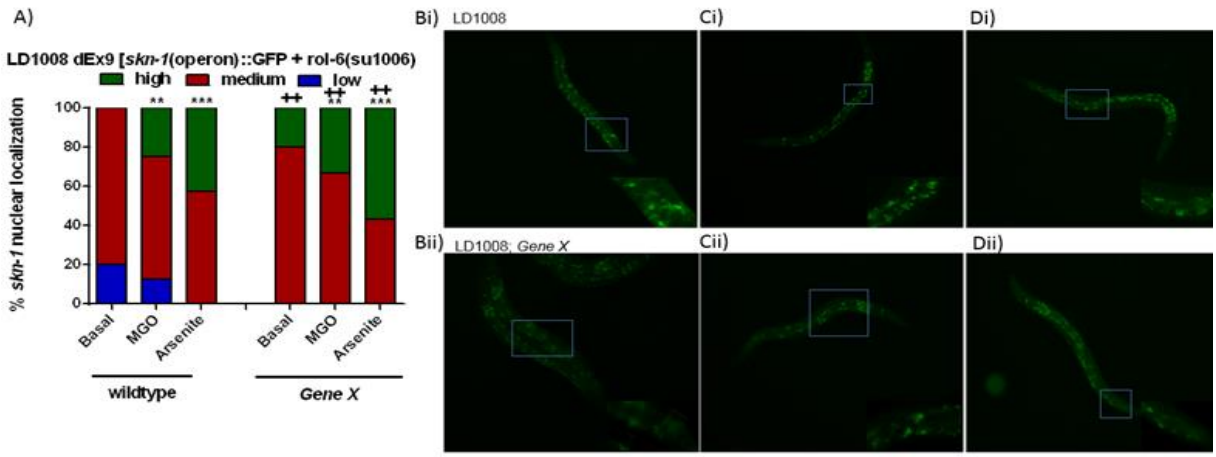

Figure 20: **Gene *X KO* enhances *skn-1* activation in oxidative stress conditions.** *skn-1* translational GFP reporter were used and data was collected at Day 1 and grown at 25˚C A) Quantification of the *skn-1* translational reporter compare to *skn-1 translational reporter with* Gene X KO in Basal, and stress conditions treated with 7mM MGO and 3mM Arsenite, N=25. All pairwise quantifications were conducted using two- tailed student t-tests. Significance was determined by p value as follows: ** <0.01. Bi) representative image of the *skn-1*:: GFP localizing in the nucleus during basal conditions. Bii) representative image of the *skn-1*:: GFP with *Gene X* KO localizing in the nucleus during basal conditions. Ci) representative image of the *skn-1*:: GFP localizing in the nucleus during treatment of MGO. Bii) representative image of the *skn-1*:: GFP with *Gene X* KO localizing in the nucleus during treatment of MGO Ci) representative image of the *skn-1*:: GFP localizing in the nucleus during treatment of Arsenite Cii) representative image of the *skn-1*:: GFP with *Gene X* KO localizing in the nucleus during treatment of Arsenite.

Next, we examined protein levels utilizing a genetically tagged GFP reporters to qualitatively examine nuclear localization of *skn-1*and its direct downstream targets. Nuclear localization was used as the qualitative readout of protein expression because as the *skn-1*, *gst-4,* and *gcs-1* proteins are activated they will translocated into the nucleus from the cytoplasm to turn on phase-II detoxification signals that lead to longevity (43). First, we examined GFP-tagged *skn-1* expression to observe qualitative changes when crossed to the *Gene X* mutation. We saw that when *Gene X* was functional there was less

nuclear localization of *skn-1* (Figure 20A). We also examined expression levels of *skn-1* when worms were raised in the stress conditions of MGO and Arsenite. We saw that as *C. elegans* were raised in both oxidative stress conditions and basal conditions, *skn-1* expression increased (Figure 20A). Subsequently, when *Gene X was* inhibited there was a significant increase in *skn-1* expression compared to the wildtype (Figure 20A, Bi, and Bii). During MGO and Arsenite stress we noticed that in the *skn-1* with *Gene X* knockout there was more nuclear localization compared to the wildtype (Figure 20A, Ci, Cii, Di, and Dii).

After determining that *Gene X* regulated protein expression of *skn-1*, we next examined gst-*4* and *gcs-1* expression. To examine protein expression, we utilized the *gst-4* and *gcs-1* transcriptional reporters tagged with GFP and examined fluorescence. Skn-*1* expression will induce transcription of downstream targets, leading to activation of the glyoxalase genes *glod-4, djr-1.1, and djr-1.2*. We observed a higher amount of fluorescence of these downstream targets when *Gene X* was inhibited by a null mutation, supporting the functional connection of *skn-1* and *Gene X.* At the same time, we looked to see if there were changes to protein levels when *Gene X* was inhibited in oxidative stress conditions. This would further confirm that *Gene X* as a regulator of *skn-1*. The data showed the amount of *gst-4* fluorescence exemplified by the nuclear localization similar to *skn-1*, when *Gene X* is inhibited in both basal conditions and with oxidative stress (Figure S4). *gcs-1* fluorescence expression led to an increased activation of fluorescence in the *Gene X* mutant compared to wildtype (Figure S5). The increase in *gst-4* and *gcs-1* nuclear localization expression supports that *Gene X* is functioning in a way that is repressing *skn-1* function. Removal of *Gene X* leads to further detoxification.

Further confirmation is needed to understand how *skn-1* protects against the diabetic and neurodegenerative pathologies and when *Gene X* is inhibited.

Identification of the functional interaction of *Gene X* and *skn-1* through the *skn-1* mutation

After looking at protein expression and nuclear localization of *skn-1* and its downstream targets with *Gene X* function, we wanted to understand the importance of *skn-1* function as it pertains to *Gene X* and the glyoxalases. *skn-1* is a key factor in the activation of the glyoxalase detoxification pathway due to *trpa-1* acting as a sensor and receptor for the free α-dicarbonyl compounds. When the free α-dcs stimulate the *trpa-1*

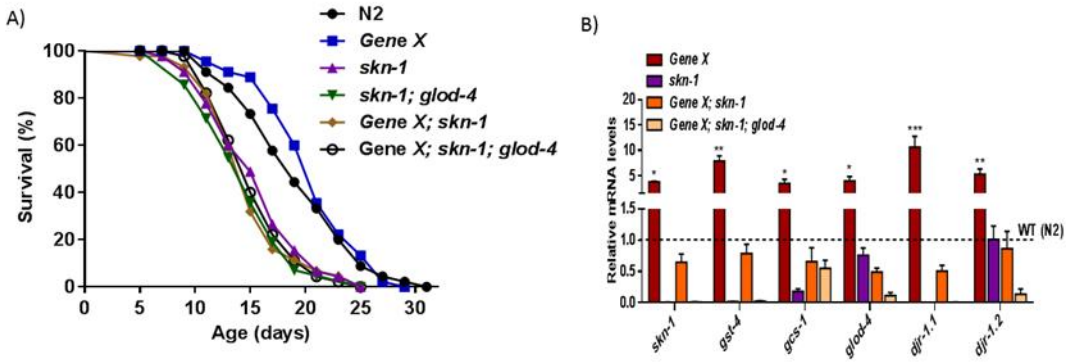

Figure 21: ***skn-1* gene is necessary for the rescue effect seen in *Gene X; glod-4.*** A) Lifespan curves of wildtype (black), *Gene X (blue), skn-1 (purple), skn-1;glod-4 (green), Gene X* ; *skn-1 (brown),* and *Gene X;skn-1; glod-4* mutant (clear) N = 45. B) All data normalized to wildtype and expression levels of *pmp-2* gene. Relative expression of *skn-1, gst-4, gcs-1, glod-4, djr-1.1,* and *djr-1.2* in *Gene X* KO, *skn-1, Gene X; skn-1,* and *Gene X; skn-1; glod-4* in basal conditions. All pairwise quantifications were conducted using two- tailed student t-tests. Significance was determined by p value as follows: * <0.5, ** <0.01, and *** <0.001. Error bar depict standard deviation in samples.

receptor, the *skn-1* gene is the key initiator of the pathway. In order to determine the role of *skn-1* we used a *skn-1* null mutant. The *skn-1* mutant was crossed to an established *Gene X; glod-4 C. elegans* model that originally exhibited a protective effect against the pathological phenotypes associated with diabetes and Parkinson's Disease. The *skn-1* null mutation caused the lifespan extension seen in *Gene X; glod-4,* to be inhibited and exhibited a similar reduction in lifespan to the skn-*1* mutant alone *(*Figure 21A). The removal of *skn-1* led to the reduction of lifespan, showing that the *skn-1* gene has a necessary role for survival. To better quantify the role that *skn-1* plays in neuronal integrity, the GFP-tagged pan-neuronal and dopaminergic reporters were crossed to the *Gene X; glod-4* mutant. We determined that *skn-1* is necessary and when mutated along with the *Gene X* mutant there was no longer protection against or rescue of disease phenotypes. In order to examine these effects, we performed a qPCR analysis examining expression of *skn-1, gst-4, gcs-1,* and the glyoxalase genes. We found that while there is an up regulation of these genes in the *Gene X* knockout, when the *skn-1* is inhibited, the genetic expression of these genes became downregulated compared to the wildtype (Figure 21B). This shows that genetic activation of *skn-1* is required for extension and alleviation of these pathological phenotypes.

Discussion:

The *glod-4* (*Glo1*) *C. elegans* knockout model demonstrated pathological phenotypes frequently observed in human patients with long term type 2 diabetes. These complications are also shown to have a strong association with the worm orthologs of *DJ1* (26), which supports the idea that PD is correlated with diabetes (9). Further evidence shows that a potential cause of the progression of these diseases could be due to

the production and accumulation of toxic compounds known as α-dicarbonyls (α-dcs) (56), which are detoxified by the glyoxalase enzymes (57). Mutations in the glyoxalase genes lead to accumulation of α-dcs that irreversibly modifies macromolecules, resulting in the formation of a class of toxic compounds known as Advance Glycation End Products (AGEs). The buildup of these compounds is strongly associated with the progression of diseases phenotypes such as age-related degradation of the neurons and increased sensitivity in touch, known as hyperesthesia (10).

To understand how neuronal degeneration and hyperesthesia are influenced by the glyoxalase genes, we acquired a *glod-4* glyoxalase knockout. We hypothesized that the resulting accumulation of α-dcs would cause increased neuronal damage, and our experiments displayed chronic degradation of the neuronal integrity exhibited by phenotypic neuronal thinning, and outgrowth/ branches (Figure 7). Additionally, the accumulation of α-dcs due to the loss of functionality in *djr-1.2*, a gene which is neuronally expressed, led to significant damages within the neuronal architecture resulting in the complete loss of dopaminergic neurons (Figure 9). These results suggest that tissue specificity of the glyoxalase genes could play a role in the modulation of damages to the neuronal architecture over time. Because of these results, we investigated pathogenic proteins related to specific neurodegenerative diseases along with their underlying causes. Within the glyoxalase mutants we saw neuronal degeneration, and that overexpressing α-synuclein, one of the main factors known to cause damages in Parkinson disease (58), exacerbated glyoxalase-driven neuronal degradation. These results revealed that there could be a potential connection between α-synuclein expression and the neuronal damage due to long term diabetes (Figure 7). Utilizing a

worm model that recapitulates some of the complications of diabetes, we found that overexpression of α-synuclein further exacerbated the damages, revealing a potential link between diabetic complications and PD. This exemplifies that inducing factors which regulate these two diseases could mediate an additive effect on healthspan.

In reviewing literature to discover potential mechanisms by which diabetes could be regulated, we came across a study which revealed novel genetic loci associated with these diabetic complications in humans (46). Utilizing an RNAi screen in a *glod-4* mutant background multiple genes were identified to exhibit phenotypic changes, with only *Gene X* RNAi exhibiting beneficial effects. In order to gain further insights into how *Gene X* RNAi rendered its function, we first examined if a mutation to *Gene X* could alleviate pathological complications in glyoxalase mutants. *Gene X* mutants in the glyoxalase mutant background not only showed an abrogation of hyperesthesia, but also led to increased lifespan in *glod-4* animals. We hypothesized that *Gene X* could be regulating the detoxification of α-dicarbonyl accumulation, and that this regulation rescues lifespan. Next, we examined if *Gene X* might play a role in alleviating stresses produced by α-dcs. We identified that with the addition of exogenous methylglyoxal (an α-dc compound), worms with a mutation to *Gene X* were resistant against α-dc stress. Our results identified that a loss of *Gene X* functionality exposes a regulatory effect on the α-dc detoxification pathway, suggesting that *Gene X* may inhibit the induction of the body's own immune response (59,60) to detoxify the accumulated pathological aggregations. However, our understanding of the effects of *Gene X* on α-dicarbonyl levels is still limited, as the process of analyzing the accumulation of these compounds through mass spectrometry is still being optimized. By testing the effects of these compounds *in vivo,* we conclude that

their accumulation exacerbates phenotypic pathologies and that loss of *Gene X* alleviates these harmful effects through regulated detoxification of these compounds.

To look at what genetic factors could be regulated by *Gene X*, we analyzed the genetic motifs to which *Gene X* can bind. A top candidate binding motif for *Gene X* was one which is shared with *skn-1*, a gene known to contribute to longevity and protect against stress (42). We hypothesized that *Gene X* and *skn-1* could *be* interacting through binding site competition at the promoter region of *skn-1* canonical targets thus repressing *skn-1* activity. This hypothesis is supported by literature that shows that *Gene X* acts as a transcriptional repressor in AWC neurons (46) within *C. elegans.* We utilized qPCR and nuclear localization activity to determine if there was a transcriptional repression of the *skn-1* by *Gene X*. Our results showed that *Gene X* mutation led to upregulated expression of downstream *skn-1* targets, exemplified by the increase in nuclear localization of the *skn-1*. These results agreed with our conclusion that *Gene X* is repressing the detoxification of α-dcs by regulating *skn-1* and its downstream targets *gst-4* and *gcs-1,* seen previously to be upstream regulators of the glyoxalase detoxification pathway (26). We also observed that alleviation of the α-dc-related phenotypes in the glyoxalase mutants was dependent on *skn-1* activity within the *Gene X* mutant, since this rescue effect was nullified when *skn-1* was mutated. This validates the role of *Gene X* in regulating *skn-1* by inhibiting its activation. However, further examination into this mechanism is needed. Future studies into this novel regulation of *skn-1* could incorporate the use of different binding assays, such as ChIP-qPCR or EMSA to examine the binding sites for *Gene X* and *skn-1* and how they inhibit each other. We conclude from these results that for the most effective detoxification of the α-dc compounds, *skn-1* must be

active and *Gene X* needs to be downregulated for the rescue of the glyoxalase pathologies to occur. Our evidence also suggests that a mutation to *Gene X* cannot produce these beneficial effects without the activation of *skn-1* to complement it by upregulating downstream targets to induce glyoxalase expression. This study delineates a novel regulation of *skn-1* via *Gene X* that improves survival by controlling the accumulation of α-dicarbonyls.

Further studies to understand the means by which *Gene X* functions, such as probable downstream targets, are necessary to better elucidate how it can modulate health and survival in the context of PD. Additional mechanistic insights influencing downstream targets of *Gene X* can be elucidated through RNA sequencing experiments. This would allow for better interpretation of how *Gene X* is functioning *in vivo*. By understanding *Gene X* function, we would be able to examine the vast array of potential therapeutics, conserved genes targets, and pathways modulating AGE-mediated neuronal damage. From this study, we uncover a pathway that could reveal a potential therapeutic target to regulate diabetic pathologies and neurodegenerative diseases, such as Parkinson's and Alzheimer's disease, by the amelioration of AGEs.

Reference

1. Katsuumi G, Shimizu I, Yoshida Y, Minamino T. Vascular Senescence in Cardiovascular and Metabolic Diseases. Front Cardiovasc Med [Internet]. 2018 Mar 5;5. Available from: http://journal.frontiersin.org/article/10.3389/fcvm.2018.00018/full

2. Bang E, Lee B, Park J-O, Jang Y, Kim A, Kim S, et al. The Improving Effect of HL271, a Chemical Derivative of Metformin, a Popular Drug for Type II Diabetes Mellitus, on Aging-induced Cognitive Decline. Exp Neurobiol [Internet]. 2018 Feb;27(1):45. Available from: https://synapse.koreamed.org/DOIx.php?id=10.5607/en.2018.27.1.45

3. Nation U. Ageing [Internet]. Global issues. [cited 2017 Aug 22]. Available from: http://www.un.org/en/sections/issues-depth/ageing/

4. Kirkman MS, Briscoe VJ, Clark N, Florez H, Haas LB, Halter JB, et al. Diabetes in Older Adults. Diabetes Care [Internet]. 2012 Dec 1;35(12):2650 LP-2664. Available from: http://care.diabetesjournals.org/content/35/12/2650.abstract

5. Mayo Clinic. Hyperglycemia in diabetes [Internet]. Disearse & Conditions. 2018 [cited 2017 Aug 22]. Available from: https://www.mayoclinic.org/diseases-conditions/hyperglycemia/symptoms-causes/syc-20373631

6. Moraru A, Wiederstein J, Pfaff D, Fleming T, Miller AK, Nawroth P, et al. Short Article Elevated Levels of the Reactive Metabolite Methylglyoxal Recapitulate Progression of Type 2 Short Article Elevated Levels of the Reactive Metabolite Methylglyoxal Recapitulate Progression of Type 2 Diabetes. Cell Metab [Internet]. 2018;27(4):926–934.e8. Available from: https://doi.org/10.1016/j.cmet.2018.02.003

7. Turton JL, Raab R, Rooney KB. Low-carbohydrate diets for type 1 diabetes mellitus: A systematic review. PLoS One [Internet]. 2018;13(3):1–16. Available from: https://doi.org/10.1371/journal.pone.0194987

8. Keller MP, Gatti DM, Schueler KL, Rabaglia ME, Stapleton DS, Simecek P, et al. Genetic Drivers of Pancreatic Islet Function. Genetics [Internet]. 2018 May;209(1):335–56. Available from: http://www.genetics.org/lookup/doi/10.1534/genetics.118.300864

9. Verdile G, Fuller SJ, Martins RN. The role of type 2 diabetes in neurodegeneration. Neurobiol Dis [Internet]. 2015;84:22–38. Available from: http://www.sciencedirect.com/science/article/pii/S0969996115001552

10. Babizhayev MA, Strokov IA, Nosikov V V., Savel'yeva EL, Sitnikov VF, Yegor EY, et al. The Role of Oxidative Stress in Diabetic Neuropathy: Generation of Free Radical Species in the Glycation Reaction and Gene Polymorphisms Encoding Antioxidant Enzymes to Genetic Susceptibility to Diabetic Neuropathy in Population of Type I Diabetic Patient. Cell Biochem Biophys [Internet].

2015;71(3):1425–43. Available from: http://dx.doi.org/10.1007/s12013-014-0365-y

11. Ma M, Xu Y, Xiong S, Zhang J, Gu Q, Ke B, et al. Involvement of ciliary neurotrophic factor in early diabetic retinal neuropathy in streptozotocin-induced diabetic rats. Eye [Internet]. 2018 May 23; Available from: http://dx.doi.org/10.1038/s41433-018-0110-7

12. Science NI of EH. Neurodegenerative diseases [Internet]. Research. 2017 [cited 2017 Aug 14]. Available from: https://www.niehs.nih.gov/research/supported/health/neurodegenerative/index.cfm

13. Joint Programe E. What is Neurodegenerative Disease? [Internet]. JPND Reasearch. 2016 [cited 2017 Aug 22]. Available from: http://www.neurodegenerationresearch.eu/about/what/

14. Cooper JF, Dues DJ, Spielbauer KK, Machiela E, Senchuk MM, Van Raamsdonk JM. Delaying aging is neuroprotective in Parkinson's Disease: a genetic analysis in C. elegans models. 2015 Nov 19;1:15022. Available from: http://dx.doi.org/10.1038/npjparkd.2015.22

15. Pomatto LCD, Davies KJA. The role of declining adaptive homeostasis in ageing. J Physiol [Internet]. 2017 Dec 15;595(24):7275–309. Available from: http://doi.wiley.com/10.1113/JP275072

16. Ayyadevara S, Balasubramaniam M, Gao Y, Yu L-R, Alla R, Shmookler Reis R. Proteins in aggregates functionally impact multiple neurodegenerative disease models by forming proteasome-blocking complexes. Aging Cell [Internet]. 2015 Feb;14(1):35–48. Available from: http://doi.wiley.com/10.1111/acel.12296

17. Ramasamy R, Vannucci SJ, Yan SS Du, Herold K, Yan SF, Schmidt AM. Advanced glycation end products and RAGE: a common thread in aging, diabetes, neurodegeneration, and inflammation. Glycobiology [Internet]. 2005;15(7):16R–28R. Available from: http://dx.doi.org/10.1093/glycob/cwi053

18. Rehman SU, Shah SA, Ali T, Chung J Il, Kim MO. Anthocyanins Reversed D-Galactose-Induced Oxidative Stress and Neuroinflammation Mediated Cognitive Impairment in Adult Rats. Mol Neurobiol [Internet]. 2017 Jan;54(1):255–71. Available from: https://doi.org/10.1007/s12035-015-9604-5

19. Li J, Liu D, Sun L, Lu Y, Zhang Z. Advanced glycation end products and neurodegenerative diseases: Mechanisms and perspective. J Neurol Sci [Internet]. 2017 Aug 22;317(1):1–5. Available from: http://dx.doi.org/10.1016/j.jns.2012.02.018

20. Ahmad S, Khan MS, Akhter F, Khan MS, Khan A, Ashraf JM, et al. Glycoxidation of Biological Macromolecules: A Critical Approach to Halt the Menace of Glycation. Glycobiology [Internet]. 2014;24(11):979–90. Available from: http://dx.doi.org/10.1093/glycob/cwu057

21. Fokkens BT, Mulder DJ, Schalkwijk CG, Scheijen JL, Smit AJ, Los LI. Vitreous advanced glycation endproducts and α-dicarbonyls in retinal detachment patients with type 2 diabetes mellitus and non-diabetic controls. PLoS One [Internet]. 2017;12(3):1–11. Available from: https://doi.org/10.1371/journal.pone.0173379

22. Lopez-Clavijo AF, Duque-Daza CA, Romero Canelon I, Barrow MP, Kilgour D, Rabbani N, et al. Study of an Unusual Advanced Glycation End-Product (AGE) Derived from Glyoxal Using Mass Spectrometry. J Am Soc Mass Spectrom [Internet]. 2014 Apr;25(4):673–83. Available from: https://doi.org/10.1007/s13361-013-0799-2

23. Zhao D, Le TT, Larsen LB, Li L, Qin D, Su G, et al. Effect of glycation derived from α-dicarbonyl compounds on the in vitro digestibility of β-casein and β-lactoglobulin: A model study with glyoxal, methylglyoxal and butanedione. Food Res Int [Internet]. 2017;102:313–22. Available from: http://www.sciencedirect.com/science/article/pii/S0963996917306877

24. Khan MA, Schultz S, Othman A, Fleming T, Lebrón-Galán R, Rades D, et al. Hyperglycemia in Stroke Impairs Polarization of Monocytes/Macrophages to a Protective Noninflammatory Cell Type. J Neurosci [Internet]. 2016;36(36):9313–25. Available from: http://www.jneurosci.org/lookup/doi/10.1523/JNEUROSCI.0473-16.2016

25. Brings S, Fleming T, Freichel M, Muckenthaler M, Herzig S, Nawroth P. Dicarbonyls and Advanced Glycation End-Products in the Development of Diabetic Complications and Targets for Intervention. Schalkwijk CG, editor. Int J Mol Sci [Internet]. 2017 May 5;18(5):984. Available from: http://www.mdpi.com/1422-0067/18/5/984

26. Chaudhuri J, Bose N, Gong J, Hall D, Rifkind A, Bhaumik D, et al. A Caenorhabditis elegans Model Elucidates a Conserved Role for TRPA1-Nrf Signaling in Reactive α-Dicarbonyl Detoxification. Curr Biol [Internet]. 2016;26(22):3014–25. Available from: http://dx.doi.org/10.1016/j.cub.2016.09.024

27. Rabbani N, Xue M, Thornalley PJ. Dicarbonyls and glyoxalase in disease mechanisms and clinical therapeutics. Glycoconj J [Internet]. 2016 Aug;33(4):513–25. Available from: https://doi.org/10.1007/s10719-016-9705-z

28. Maessen DE, Hanssen NM, Scheijen JL, van der Kallen CJ, van Greevenbroek MM, Stehouwer CD, et al. Post–Glucose Load Plasma α-Dicarbonyl Concentrations Are Increased in Individuals With Impaired Glucose Metabolism and Type 2 Diabetes: The CODAM Study. Diabetes Care [Internet]. 2015 May 1;38(5):913 LP-920. Available from: http://care.diabetesjournals.org/content/38/5/913.abstract

29. Jack M, Wright D. Role of advanced glycation endproducts and glyoxalase I in diabetic peripheral sensory neuropathy. Transl Res [Internet]. 2012 May;159(5):355–65. Available from:

http://linkinghub.elsevier.com/retrieve/pii/S1931524411004312

30. Jandial R, Neman J, Lim P, Tamae D, Kowolik C, Wuenschell G, et al. Inhibition of GLO1 in Glioblastoma Multiforme Increases DNA-AGEs, Stimulates RAGE Expression, and Inhibits Brain Tumor Growth in Orthotopic Mouse Models. Int J Mol Sci [Internet]. 2018 Jan 30;19(2):406. Available from: http://www.mdpi.com/1422-0067/19/2/406

31. Brouwers O, Niessen PM, Ferreira I, Miyata T, Scheffer PG, Teerlink T, et al. Overexpression of Glyoxalase-I Reduces Hyperglycemia-induced Levels of Advanced Glycation End Products and Oxidative Stress in Diabetic Rats. J Biol Chem [Internet]. 2011 Jan 14;286(2):1374–80. Available from: http://www.jbc.org/lookup/doi/10.1074/jbc.M110.144097

32. Distler MG, Palmer AA. Role of Glyoxalase 1 (Glo1) and methylglyoxal (MG) in behavior: recent advances and mechanistic insights. Front Genet [Internet]. 2012;3:250. Available from: http://journal.frontiersin.org/article/10.3389/fgene.2012.00250/abstract

33. Rifkind A. Modeling Therapeutic Strategies for Diabetic Pathologies. Master's Theses Capstone Proj [Internet]. 2016;227. Available from: https://scholar.dominican.edu/masters-theses/227/

34. Yang Y-W, Hsieh T-F, Li C-I, Liu C-S, Lin W-Y, Chiang J-H, et al. Increased risk of Parkinson disease with diabetes mellitus in a population-based study. Arias-Carrion. O, editor. Medicine (Baltimore) [Internet]. 2017 Jan;96(3):e5921. Available from: http://content.wkhealth.com/linkback/openurl?sid=WKPTLP:landingpage&an=00005792-201701200-00030

35. Li J-Q, Tan L, Yu J-T. The role of the LRRK2 gene in Parkinsonism. Mol Neurodegener [Internet]. 2014;9(1):47. Available from: http://molecularneurodegeneration.biomedcentral.com/articles/10.1186/1750-1326-9-47

36. Sietske N. Heyn, PhD, Charles Patrick Davis, MD P. Parkinson's Disease Symptoms, Signs, Causes, Stages, and Treatment [Internet]. MedicineNet.com. 2018 [cited 2017 Aug 22]. Available from: https://www.medicinenet.com/parkinsons_disease/article.htm#what_is_parkinsons_disease

37. Lee J, Song J, Kwon K, Jang S, Kim C, Baek K, et al. Human DJ-1 and its homologs are novel glyoxalases. Hum Mol Genet [Internet]. 2012 Jul 15;21(14):3215–25. Available from: http://dx.doi.org/10.1093/hmg/dds155

38. trpa-1 (gene) - WormBase : Nematode Information Resource [Internet]. Wormbase. [cited 2017 Sep 23]. Available from: http://www.wormbase.org/species/c_elegans/gene/WBGene00007801#0-9g-3

39. Corsi AK, Wightman B, Chalfie MA. Transparent window into biology: A primer on Caenorhabditis elegans The C. elegans Research Community [Internet]. 2015. 1551-8507 p. Available from: http://www.wormbook.org/chapters/www_celegansintro/celegansintro.html

40. Fire A, Xu S, Montgomery MK, Kostas SA, Driver SE, Mello CC. Potent and specific genetic interference by double-stranded RNA in Caenorhabditis elegans. Nature [Internet]. 1998 Feb 19;391(6669):806–11. Available from: http://www.nature.com/articles/35888

41. Nummenmaa E, Hämäläinen M, Moilanen LJ, Paukkeri E-L, Nieminen RM, Moilanen T, et al. Transient receptor potential ankyrin 1 (TRPA1) is functionally expressed in primary human osteoarthritic chondrocytes. Arthritis Res Ther [Internet]. 2016 Dec 11;18(1):185. Available from: http://arthritis-research.biomedcentral.com/articles/10.1186/s13075-016-1080-4

42. Blackwell TK, Steinbaugh MJ, Hourihan JM, Ewald CY, Isik M. SKN-1/Nrf, stress responses, and aging in Caenorhabditis elegans. Free Radic Biol Med [Internet]. 2015 Nov;88(Pt B):290–301. Available from: http://linkinghub.elsevier.com/retrieve/pii/S0891584915002762

43. Detienne G, Van de Walle P, De Haes W, Schoofs L, Temmerman L. SKN-1-independent transcriptional activation of glutathione S-transferase 4 (GST-4) by EGF signaling. Worm [Internet]. 2016 Aug 31;5(4):e1230585. Available from: http://www.pubmedcentral.nih.gov/articlerender.fcgi?artid=PMC5190145

44. Liao VH-C, Yu C-W. Caenorhabditis elegans gcs-1 Confers Resistance to Arsenic-Induced Oxidative Stress. Biometals [Internet]. 2005 Oct;18(5):519–28. Available from: https://doi.org/10.1007/s10534-005-2996-3

45. Leiers B, Kampkötter A, Grevelding CG, Link CD, Johnson TE, Henkle-Dührsen K. A stress-responsive glutathione S-transferase confers resistance to oxidative stress in Caenorhabditis elegans. Free Radic Biol Med [Internet]. 2003;34(11):1405–15. Available from: http://www.sciencedirect.com/science/article/pii/S0891584903001023

46. Ma RC. Genetics of cardiovascular and renal complications in diabetes. J Diabetes Investig [Internet]. 2016 Mar;7(2):139–54. Available from: http://doi.wiley.com/10.1111/jdi.12391

47. Lesch BJ, Bargmann CI. The homeodomain protein hmbx-1 maintains asymmetric gene expression in adult C. elegans olfactory neurons. Genes Dev [Internet]. 2010 Aug 15;24(16):1802–15. Available from: http://genesdev.cshlp.org/cgi/doi/10.1101/gad.1932610

48. Stefanis L. -Synuclein in Parkinson's Disease. Cold Spring Harb Perspect Med [Internet]. 2012 Feb 1;2(2):a009399–a009399. Available from: http://perspectivesinmedicine.cshlp.org/lookup/doi/10.1101/cshperspect.a009399

49. Feng X, Luo Z, Jiang S, Li F, Han X, Hu Y, et al. The telomere-associated homeobox-containing protein TAH1/HMBOX1 participates in telomere maintenance in ALT cells. J Cell Sci [Internet]. 2013;126(17):3982–9. Available from: http://jcs.biologists.org/content/126/17/3982

50. Stiernagle T. Maintenance of C. elegans [Internet]. The C. elegans Research Community; 2006. 1551-8507 p. Available from: http://www.wormbook.org/chapters/www_strainmaintain/strainmaintain.html

51. Hobert O, Moerman DG, Clark KA, Beckerle MC, Ruvkun G. A conserved LIM protein that affects muscular adherens junction integrity and mechanosensory function in Caenorhabditis elegans. J Cell Biol [Internet]. 1999 Jan 11;144(1):45–57. Available from: http://www.pubmedcentral.nih.gov/articlerender.fcgi?artid=PMC2148118

52. Skallerup Andersen M, Karshenas A, Winther Bach F, Gazerani P. Pain and Sensory Abnormalities in Parkinson's Disease—An Age- and Gender-matched Controlled Pilot Study. US Neurol [Internet]. 2015;11(01):27. Available from: http://www.touchneurology.com/articles/pain-and-sensory-abnormalities-parkinson-s-disease-age-and-gender-matched-controlled-pilot

53. Chen X, Barclay JW, Burgoyne RD, Morgan A. Using C. elegans to discover therapeutic compounds for ageing-associated neurodegenerative diseases. Chem Cent J [Internet]. 2015 Nov;9(1):65. Available from: https://doi.org/10.1186/s13065-015-0143-y

54. Ray A, Martinez BA, Berkowitz LA, Caldwell GA, Caldwell KA. Mitochondrial dysfunction, oxidative stress, and neurodegeneration elicited by a bacterial metabolite in a C. elegans Parkinson's model. Cell Death Dis [Internet]. 2014;5(1):e984-12. Available from: http://dx.doi.org/10.1038/cddis.2013.513

55. Consortium TEP. An integrated encyclopedia of DNA elements in the human genome. Nature [Internet]. 2012 Sep 5;489:57. Available from: http://dx.doi.org/10.1038/nature11247

56. Maher P, Dargusch R, Ehren JL, Okada S, Sharma K, Schubert D. Fisetin Lowers Methylglyoxal Dependent Protein Glycation and Limits the Complications of Diabetes. Deli MA, editor. PLoS One [Internet]. 2011 Jun 27;6(6):e21226. Available from: http://dx.plos.org/10.1371/journal.pone.0021226

57. Ahmed N, Thornalley PJ, Dawczynski J, Franke S, Strobel J, Stein G, et al. Methylglyoxal-Derived Hydroimidazolone Advanced Glycation End-Products of Human Lens Proteins. Investig Opthalmology Vis Sci [Internet]. 2003;44(12):5287. Available from: http://iovs.arvojournals.org/article.aspx?doi=10.1167/iovs.03-0573

58. Abul Khair SB, Dhanushkodi NR, Ardah MT, Chen W, Yang Y, Haque ME. Silencing of Glucocerebrosidase Gene in Drosophila Enhances the Aggregation of Parkinson's Disease Associated α-Synuclein Mutant A53T and Affects Locomotor

Activity. Front Neurosci [Internet]. 2018 Feb 16;12. Available from: http://journal.frontiersin.org/article/10.3389/fnins.2018.00081/full

59. Wu L, Zhang C, Zheng X, Tian Z, Zhang J. HMBOX1, homeobox transcription factor, negatively regulates interferon-γ production in natural killer cells. Int Immunopharmacol [Internet]. 2011;11(11):1895–900. Available from: http://dx.doi.org/10.1016/j.intimp.2011.07.021

60. Wu L, Zhang C, Zhang J. HMBOX1 negatively regulates NK cell functions by suppressing the NKG2D/DAP10 signaling pathway. Cell Mol Immunol [Internet]. 2011 Sep 27;8(5):433–40. Available from: http://www.pubmedcentral.nih.gov/articlerender.fcgi?artid=PMC4012885

61. Van den Born JC, Hammes H-P, Greffrath W, van Goor H, Hillebrands J-L. Gasotransmitters in Vascular Complications of Diabetes. Diabetes [Internet]. 2016;65(2):331–45. Available from: http://diabetes.diabetesjournals.org/lookup/doi/10.2337/db15-1003

62. Rabbani N, Thornalley PJ. Dicarbonyl stress in cell and tissue dysfunction contributing to ageing and disease. Biochem Biophys Res Commun [Internet]. 2015;458(2):221–6. Available from: http://dx.doi.org/10.1016/j.bbrc.2015.01.140

63. Matsuda N, Kimura M, Queliconi BB, Kojima W, Mishima M, Takagi K, et al. Parkinson's Disease-related DJ-1 functions in thiol quality control against aldehyde attack in vitro . Sci Rep [Internet]. 2017;7(1):12816. Available from: https://doi.org/10.1038/s41598-017-13146-0

64. Hasim S, Hussin NA, Alomar F, Bidasee KR, Nickerson KW, Wilson MA. A Glutathione-independent Glyoxalase of the DJ-1 Superfamily Plays an Important Role in Managing Metabolically Generated Methylglyoxal in Candida albicans. J Biol Chem [Internet]. 2014 Jan 17;289(3):1662–74. Available from: http://www.jbc.org/lookup/doi/10.1074/jbc.M113.505784

Supplementary Figures:

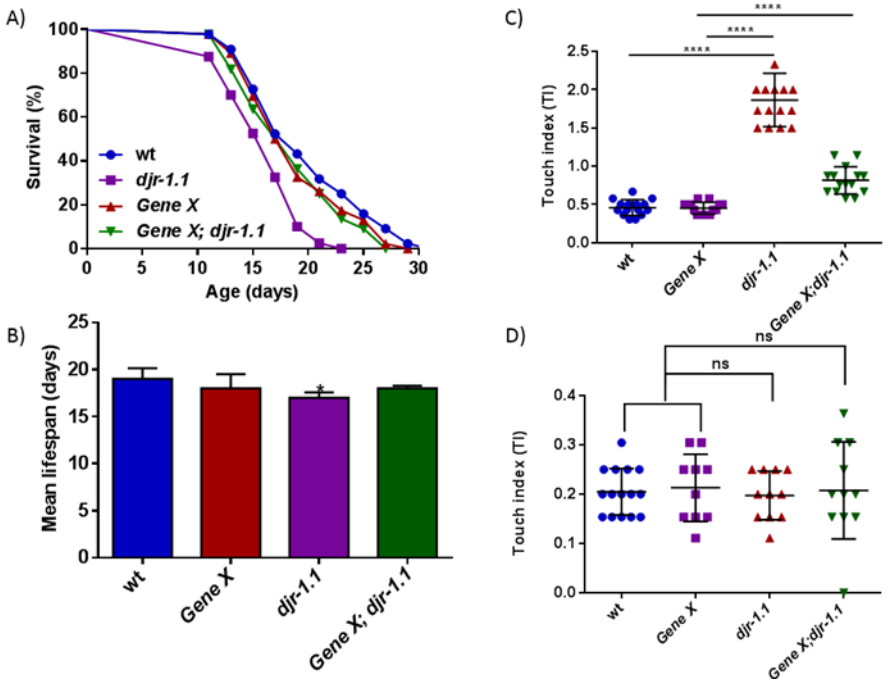

Figure S1: ***Gene X KO* protects against diabetic complications in *djr-1.1* mutant.** Error bar depict standard deviation between worms. A) Lifespan curve (Top) wildtype (blue), *Gene X* mutant (red), *djr-1.1* mutant (purple), and *Gene X; djr-1.1* mutant (green), N = 45. B) Quantification of mean lifespan. C) Hyperesthesia assay at L4 stage, N=15 D) Hyperesthesia assay at day 7, N=15 All pairwise quantifications were conducted using two- tailed student t-tests. Significance was determined by p value as follows: * <0.5, **** <0.0001, and ns: no significant difference.

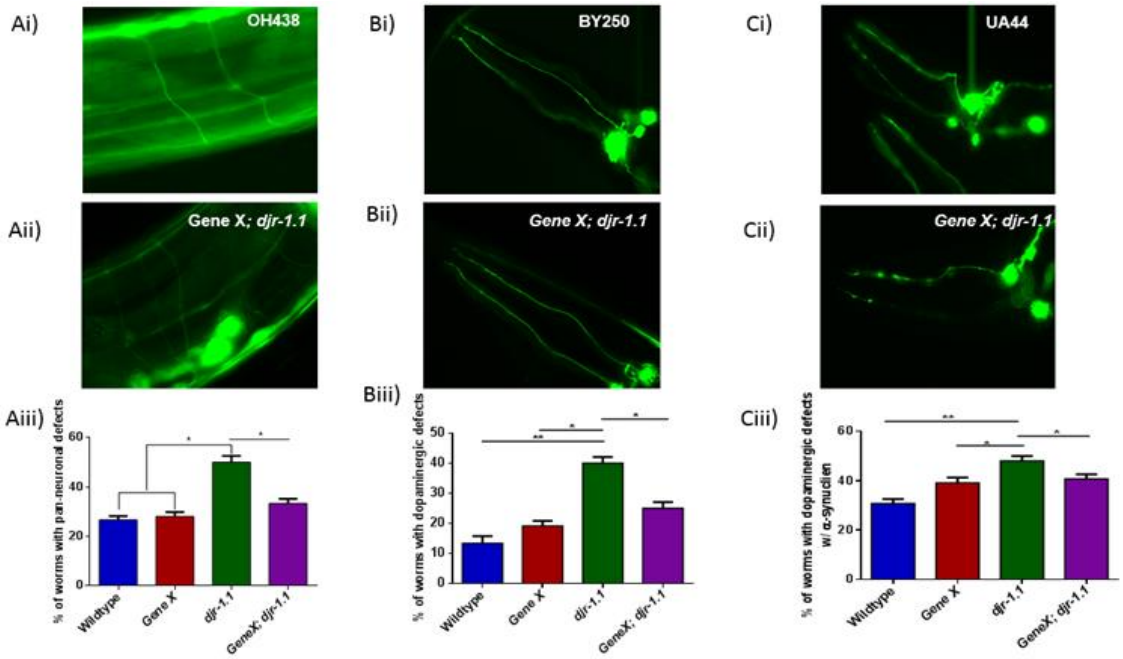

Figure S2: **Neurodegeneration utilizing the wildtype and *Gene X; djr-1.1* mutant.** Three independent GFP reporters were used and data was collected at Day 7. Ai) OH438 Pan-neuronal image of *wildtype.* Aii) Pan-neuronal image of *Gene X; djr-1.1* mutant. Aiii) quantification of neuronal damages of *Gene X; djr-1.1* mutant's pan-neuronal neuron, N= 25. Bi) BY250 Dopaminergic neuronal images of wildtype. Bii) Dopaminergic neuronal images of *Gene X; djr-1.1* mutant. Biii) quantification of neuronal damages of *G*ene X; *djr-1.1* mutant's dopaminergic neuron (BY250), N= 25. Ci) UA44 Dopaminergic neuronal images with α-synuclein expression of wildtype. Cii) Dopaminergic neuronal images with α-synuclein expression of *Gene X; djr-1.1* mutant. Ciii) quantification of neuronal damages of *Gene X; djr-1.1* mutant's dopaminergic neurons with α-synuclein expression (UA44), N= 25. All pairwise quantifications were conducted using two- tailed student t-tests. Significance was determined by p value as follows: * <0.5 and ** <0.01

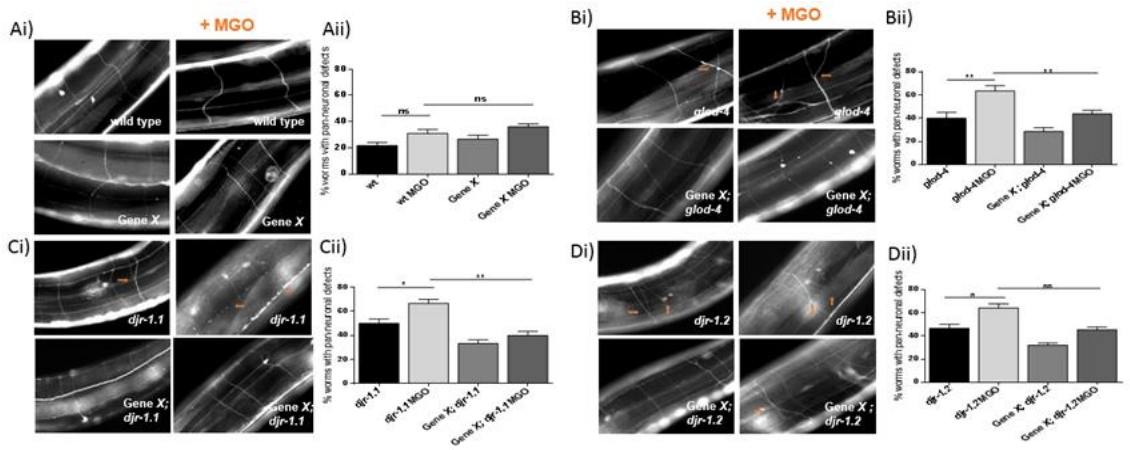

Figure S3: **Neurodegeneration inducing oxidative stress utilizing exogenous MGO.** Pan-neuronal GFP reporters were used and data was collected at Day 7, N= 20. Ai) Pan-neuronal images of wildtype, *Gene X*, wildtype +MGO, and *Gene X +MGO.* Aii) quantification of pan- neuronal damages for the *Gene X* on basal and treatment of MGO. Bi) Pan-neuronal images of *glod-4*, *Gene X; glod-4*, *glod-4* +MGO, and *Gene X; glod-4 +MGO.* Bii) Quantification of pan- neuronal damages for the *Gene X; djr-1.2* on basal and treatment of MGO. Ci) Pan-neuronal images of *djr-1.1*, *Gene X; djr-1.1*, *djr-1.1* +MGO, and *Gene X; djr-1.1 +MGO.* Cii) quantification of pan- neuronal damages for the *Gene X; djr-1.1* on basal and treatment of MGO. Di) Pan-neuronal images of *djr-1.2*, *Gene X; djr-1.2*, *djr-1.2* +MGO, and *Gene X; djr-1.2 +MGO.* Dii) quantification of pan- neuronal damages for the *Gene X; djr-1.2* on basal and treatment of MGO. All pairwise quantifications were conducted using two- tailed student t-tests. Significance was determined by p value as follows: * <0.5, ** <0.01, and ns: no significant difference.

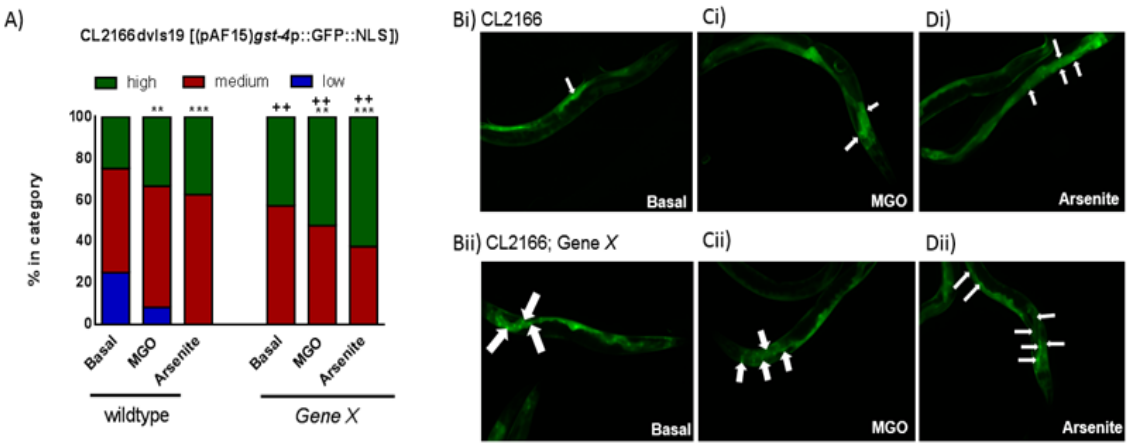

Figure S4: **Gene *X KO* enhances *gst-4* activation in oxidative stress.** *gst-4* transcriptional GFP reporter with nuclear localization signal were used and data was collected at Day 1 and grown at 25˚C. A) Quantification of the *gst-4 transcriptional* reporter compare to *gst-4 transcriptional reporter with* Gene X KO in basal, and stress conditions treated with 7mM MGO and 3mM Arsenite, N=25. All pairwise quantifications were conducted using two- tailed student t-tests. Significance was determined by p value as follows: ** <0.01. Bi) Representative image of the *gst-4p*:: GFP localizing in the nucleus during basal conditions. Bii) Representative image of the *gst-4p*:: GFP with *Gene X* KO localizing in the nucleus during basal conditions. Ci) Representative image of the *gst-4p*:: GFP localizing in the nucleus during treatment of MGO. Cii) Representative image of the *gst-4p*:: GFP with *Gene X* KO localizing in the nucleus during treatment of MGO. Di) Representative image of the *gst-4p*:: GFP localizing in the nucleus during treatment of Arsenite. Dii) Representative image of the *gst-4p*:: GFP with *Gene X* KO localizing in the nucleus during treatment of Arsenite.

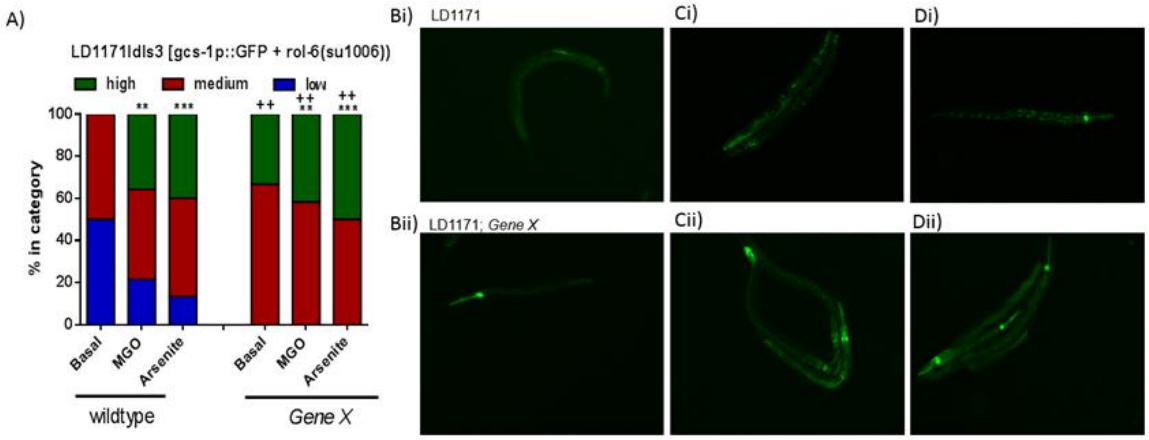

Figure S5: **Gene *X KO* enhances *gcs-1* activation in oxidative stress conditions.** *gcs-1* transcriptional GFP reporter were used and data was collected at Day 1 and grown at 25˚C. A) Quantification of the *gcs-1* transcriptional reporter compare to *gcs-1* transcriptional *reporter with* Gene X KO in basal, and stress conditions treated with 7mM MGO and 3mM Arsenite, N=25. All pairwise quantifications were conducted using two- tailed student t-tests. Significance was determined by p value as follows: ** <0.01. Bi) Representative image of the *gcs-1p*:: GFP fluorescence during basal conditions. Bii) Representative image of the *gst-1p*:: GFP with *Gene X* KO fluorescence during basal conditions. Ci) Representative image of the *gcs-1p*:: GFP fluorescence during treatment of MGO. Cii) Representative image of the *gcs-1p*:: GFP with *Gene X* KO fluorescence during treatment of MGO. Di) Representative image of the *gcs-1p*:: GFP fluorescence during treatment of Arsenite. Dii) Representative image of the *gcs-1p*:: GFP with *Gene X* KO fluorescence during treatment of Arsenite.